This is an open access article published under an ACS AuthorChoice License, which permits copying and redistribution of the article or any adaptations for non-commercial purposes.

ACS OMEGA

Article

Cite This: ACS Omega 2020, 5, 430−447

http://pubs.acs.org/journal/acsodf

Dynamics of Monolayer Physisorption in Homogeneous Mesoporous Media

Paul Papatzacos*

Department of Mathematics and Physics, University of Stavanger, 4036 Stavanger, Norway

ABSTRACT: A model for monolayer physisorption of a one-component gas on the pore surface of a homogeneous macroporous or mesoporous porous medium is presented. It originates from an averaging over many pores of a macroporous medium filled with a one-component fluid. The resulting model does not assume anything about pore shape, but assumes that the pores are so large that capillary condensation does not occur. Mathematically, the model gives coverage as the solution of an ordinary, first-order, differential equation, where the time derivative of coverage is proportional to the difference between the chemical potential of the adsorbate and the chemical potential of the ambient gas. Coverage is determined by the ambient gas density, with temperature, adsorbate critical temperature, and the Henry adsorption constant as parameters. The rest of this abstract describes what is deduced from the equations of the model. Adsorbate phase transitions are built into the model by the use of van der Waals equations of state. Equilibrium isotherms are derived from the equality of the chemical potentials. The differential equation for coverage makes it possible to determine the mathematical stability of the equilibrium isotherms, and a number of properties of the isotherms are derived, the most important being as follows: (i) an adsorbate phase transition is always accompanied by a well-defined hysteresis loop, although "loop" is somewhat misleading as its vertical boundaries do not consist of equilibrium states; (ii) the vertical boundaries are exactly located; (iii) the upper and lower boundaries consist of states that are mathematically stable, while being either physically stable or metastable, and if physical metastability is the case, then the actual state of the adsorbate (mono- or bi-phasic) will not be visible on the equilibrium isotherm. The shapes of the equilibrium isotherms are largely determined by the value of the Henry constant, whether the isotherms are subcritical or supercritical. Expressions for the location of an equilibrium isotherm's region of fastest variation and for the locations of the vertical boundaries of its hysteresis loop are found that also show the importance of Henry's constant. Dynamical, that is, time-dependent isotherms are presented for the case describing the variation of coverage resulting from forcing the ambient gas to undergo a compression−decompression loop. Two subcases are considered: the subcritical and the supercritical adsorbate. It is shown that coverage in terms of ambient pressure exhibits closed loops, even in supercritical isotherms. However, supercritical loops shrink when the cycle time increases, reminiscent of rate-dependent hysteresis observed in piezoelectricity. The model is used to interpret two experiments on the sorption of CO_2 and CH_4 on coal that showed hysteresis loops in isotherms of supercritical adsorbates and that were originally interpreted as leading to different Henry constants for adsorption and for desorption. The interpretation set forth here uses the inherent dynamics of the model and looks at the loop as just one isotherm evolving in time, thus leading to a unique Henry constant.

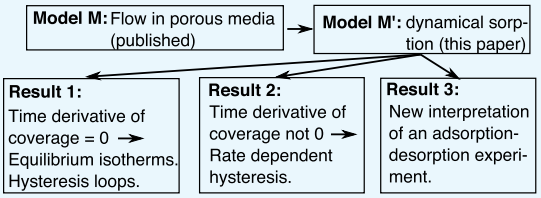

Downloaded via UNIV OF STAVANGER on January 23, 2020 at 13:24:32 (UTC).
See https://pubs.acs.org/sharingguidelines for options on how to legitimately share published articles.

1. INTRODUCTION

In experiments on gas physisorption, one often observes a discontinuity in the equilibrium isotherms and a hysteresis loop. See Morishige and Shikimi[1] and references given there. The step and the loop occur at temperatures well below the critical temperature of the ambient gas, and at pressures well below its saturation pressure.

It has been shown by Hill, in an article published in 1947,[2] that hysteresis can be explained by assuming the existence of metastable adsorbed states in monolayer physisorption, no assumptions about the pores being necessary. Hill's result is generalized in the present article, where monolayer physisorption is used to the exclusion of other processes. It must be mentioned that monolayer physisorption in a mesoporous or macroporous medium is, in a certain sense, in a class by itself, possibly together with multilayer physisorption if the number of layers is on the order of two or three. It has indeed been shown[3] that the size of the pore surface per unit volume of a mesoporous or macroporous medium is such that the amount adsorbed by monolayer physisorption is negligibly small when compared to the amount that flows in the pores. On the other hand, physisorption by capillary condensation and/or chemisorption deal with adsorbed amounts that differ by orders of magnitude from those occurring in monolayer physisorption and are essential to describe such processes as industrial hydrocarbon recovery. Capillary condensation and chemisorption are not considered in any detail in this article.

The generalization of Hill's result is done in the framework of a sorption model, called M′ for convenience here. M′, a special case of a model M to be described presently, expresses

Received: September 11, 2019
Accepted: November 27, 2019
Published: December 24, 2019

© 2019 American Chemical Society

DOI: 10.1021/acsomega.9b02956
ACS Omega 2020, 5, 430−447

the *rate of change of coverage* in terms of the coverage itself, of the ambient gas density, of temperature, of the critical temperatures of adsorbate and ambient gas, and of Henry's adsorption constant. This is not the first appearance of an equation for the rate of change of coverage (see Alfé and Gillan[4]), but it is, to the author's knowledge, the first time such an equation leads to an understanding of hysteresis loops in adsorption, and to a reinterpretation of experimental results. The three paragraphs below are short presentations of results that are described in more detail in Sections 2, 3, and 4.

The first result concerns the placement of the vertical boundaries of the hysteresis loop (Section 2.5). Ball and Evans,[5] in their article on the mechanism for hysteresis, noted that the existence of physically metastable states will bring about a transition to a physically stable state at some ambient pressure and thus produce a vertical boundary for the hysteresis loop at that pressure in adsorption as well as in desorption. They also remarked that determining the transition pressure is beyond the scope of an equilibrium theory, given that there are infinitely many physically metastable states. Now M′ describes the evolution of isotherms with time, and it also determines the equilibrium isotherms. This implies that the mathematical stability of any point on an equilibrium isotherm can be found, and it turns out that physically metastable states are mathematically stable, except for just two such points, one for adsorption and one for desorption: these are mathematically unstable and determine the transition pressures.

The second result concerns the new possibility implied by the ability of M′ to describe time-dependent isotherms. This has a direct relevance to measurements where adsorption and desorption follow different paths that join at a low and a high coverage, thus exhibiting a loop[7,6] with no vertical boundaries. The explanation given by M′ is the one given by other workers: a genuine hysteresis loop must have two vertical boundaries, so their absence is explained by appealing to an insufficient equilibration time[6] or waiting time.[8] There is, however, a new possibility implied by the ability of M′ to describe time-dependent isotherms: that of considering the noncoinciding adsorption and desorption paths as being just one isotherm evolving in time under the application of a pressure-cycle consisting of compression followed by decompression of the ambient gas. The isotherms resulting from such a cycle are shown in Section 3, for the two cases of a supercritical and a subcritical isotherm.

The third result concerns the interpretation of experiments on sorption of methane (important as a source of energy) and on sorption of carbon dioxide (an important product to sequestrate). These two cases of sorption are exceptional in that they cannot be described in the framework of capillary condensation: the critical temperatures of the substances are low compared to storage temperatures, so that capillary condensation cannot occur. Wang et al.[9] enumerate, and give references for, the hypotheses that have been made to explain the mechanism of methane and carbon dioxide sorption hysteresis: residual moisture in coal samples, surface geometry heterogeneity, chemical interaction, structural deformation, experimental inaccuracies, and insufficient waiting time. They conclude that the mechanism remains an open question. The most straightforward way to describe CH_4 and CO_2 sorption has been to use the Langmuir model: see Jessen et al.[7] See also Wang et al.[9] who look at two additional isotherms, one from the Dubinin–Radushkevich model and one from the dual sorption model, the latter allowing the inclusion of the effect of coal swelling. Section 4 of the present article gives an alternative description, based on the second result above, that leads to a unique value for the Henry constant instead of the two obtained by fitting separate equilibrium isotherms, one for adsorption and another for desorption.[7]

It is also worth mentioning that the mathematical expression of M′ is simple enough to allow approximate expressions for a number of useful quantities, such as the pressure at which the isotherm is steepest and the width of the hysteresis loop.

A short description of model M′ and of the underlying model M, follows.

M is a model for multiphase flow in a porous medium, based on the diffuse interface assumption.[10] It is the result of an averaging over many pores of the equations describing Navier–Stokes flow in the pores. The averaging leads to a new set of equations involving averaged quantities such as density, velocity components, temperature, internal energy, and entropy. M, and thereby M′, are based on the following assumptions: (a1) the fluid-containing pores are connected; (a2) the smallest pore-throat diameter is large when compared to the average distance between fluid molecules, and also when compared to their mean free path; (a3) adsorption occurs by physisorption; (a4) adsorption is monolayer; (a5) the heat generally released by adsorption does not appreciably change the temperature; (a6) the averaged fluid quantities obey the same thermodynamical laws as the quantities of the original fluid and, in particular, the averaged fluid has a well-defined pressure obeying an equation of state that can be chosen among the known ones.

M′ contains three additional assumptions: (a7) the averaged adsorbed fluid is assumed to have the thermodynamics of a two-dimensional fluid with, in particular, a spreading pressure (the negative of the surface tension)[11] obeying a van der Waals equation of state; (a8) the ambient fluid is monophasic; (a9) any externally applied changes, such as compressions or decompressions, are done so slowly that the ambient fluid velocity is negligibly small.

The consequences of these assumptions are discussed presently, after the introduction of the basic equations of M′. These are obtained directly from M (see eq 17 in Papatzacos[10]), with a slight modification in notation

$$\dot{c}_\Sigma = -\Delta\mu \tag{1}$$

$$\Delta\mu = L(\mu_\Sigma - \mu_f) \tag{2}$$

The dot in the first equation denotes partial differentiation with respect to time. A space dependence can also be included for c_Σ, but is ignored here, as it is shown below that the assumptions of model M′ make it redundant. At the level of model M, μ_f is the chemical potential of the ambient fluid, modified by the addition of two terms: a term proportional to the Laplacian of the ambient fluid density and a term proportional to the squared modulus of the ambient fluid velocity. The Laplacian originates in the diffuse interface framework, where large gradients of density exist in the interfaces between phases, if two phases coexist. The squared velocity accounts for the kinetic energy exchanged between ambient and adsorbed fluids. The two equations above are the core of model M′. They lead, after some preliminaries presented as background material in Section 5, to a differential equation for the coverage, presented in Section 5.4.

The consequences of assumptions (a1) to (a9) are as follows.

DOI: 10.1021/acsomega.9b02956
ACS Omega 2020, 5, 430−447

As a result of the averaging process, the individual characteristics of the pores are lost, leaving only two parameters to characterize the medium as a whole, which are porosity and pore surface per unit volume.[10]

Assumptions (a1), (a2), and (a4) imply that adsorption does not affect the basic description of the ambient fluid by the equations of fluid mechanics expressing balance of mass, momentum, energy, and entropy. They also imply that adsorption induces negligible changes in the values of porosity and pore surface per unit volume. In fact, assumption (a4) implies, as stated above, that inside an arbitrary volume of porous medium, the total mass adsorbed is negligibly small when compared to the mass of fluid that can flow freely in the pores.[3] Assumption (a5) implies that the quantities characterizing the ambient fluid, such as its density and temperature and consequently its pressure and chemical potential, are not modified by sorption. (On the other hand, the quantities characterizing the adsorbed fluid are determined by the ambient fluid.) Assumption (a7) implies that phase transitions can occur in the adsorbate. Assumption (a8) implies that no interfaces exist in the ambient fluid, so that the Laplacian of the ambient density that modifies the chemical potential is negligible. Assumption (a9) implies that the other term modifying the chemical potential of the ambient fluid is negligibly small. With these last two assumptions, μ_f is the usual chemical potential of the ambient fluid. Another consequence of (a8) and (a9) is that eqs 1 and 2 are space independent.

It is here emphasized that, as already mentioned, isotherm properties deduced in M′, like adsorbate phase transitions or hysteresis loops, do not depend on assumptions about the shape of the pores and, in particular, occur without the occurrence of capillary condensation.

The thermodynamical description of the fluids is given as background material in Section 5, where explicit expressions for the pressure, spreading pressure, and chemical potentials are given, and where Henry's adsorption constant is introduced. As already mentioned, the adsorbate is a van der Waals fluid, whereas three alternatives are considered for the ambient fluid: ideal with zero volume particles (called ideal type 0), ideal with nonzero volume particles (called ideal type 1), and van der Waals. The $\Delta\mu$ of eqs 1 and 2 above is then derived as a function of coverage, ambient density, and some parameters that include temperature and Henry's constant. The concepts of physical stability, metastability, and instability, known to occur in connection with the van der Waals equation of state, are illustrated in figures in the same section, for easy reference in the rest of the article.

The derivation of the basic differential equation defining M′ is given as background material in Section 5.4. Other basic properties of M′, specifically the definitions of equilibrium isotherms and of mathematical stability are given in Section 2.

2. RESULT AND DISCUSSION 1: THEORY OF EQUILIBRIUM ISOTHERMS

Equilibrium isotherms are defined in Section 2.1. Mathematical stability is defined in Section 2.2, and is followed by a section on equilibrium isotherms given by analytical expressions, then by two sections on equilibrium isotherms given by numerical solutions.

2.1. Definition of an Equilibrium Isotherm. It is here referred to Section 5.4, where the differential equation giving the time rate of change of coverage is deduced, that is, eq 59. The equilibrium isotherms follow from this equation: they are the solutions that have zero rate of change. There are additional requirements concerning stability and unicity: see the last paragraph but one of this section.

An equilibrium solution is defined as follows. Given $\tilde{T}$, $\tilde{T}_{\Sigma c}$, and ψ, an equilibrium solution of eq 59 is a set of points (r_e, θ_e) in a Cartesian plane, satisfying $0 < r_e \leq r_g$, $0 < \theta_e < 1$, and

$$\Delta\tilde{\mu}(\theta_e, r_e, \tilde{T}, \tilde{T}_{\Sigma c}, \psi) = 0 \tag{3}$$

An equivalent form of eq 3 is found as follows. The equation is first rewritten as $\tilde{\mu}_{\Sigma,\mathrm{red}} - \tilde{T} \ln \tilde{K}_H = \tilde{\mu}_{f,\mathrm{red}}$, by using eqs 56 and 57. Dividing both sides by $\tilde{T}$, exponentiating, and referring to eq 45, one finds

$$\tilde{f}_\Sigma(\theta, \tilde{T}, \tau) = \tilde{K}_H \tilde{f}_f(r, \tilde{T}) \tag{4}$$

This equation, with another definition for the proportionality constant, is identical with eq 4 in the article by Hoory and Prausnitz.[12]

Equations 3 and/or 4 give equilibrium isotherms provided that (i) points that represent mathematically and/or physically unstable states are discarded, and that (ii) non-unicity of θ_e for any r_e agrees with observations of hysteresis.

Physical stability is considered in Section 5.1; mathematical stability is defined in Section 2.2.

2.2. Mathematical Stability of Equilibrium Isotherms. Mathematical stability, or *m*-stability, of equilibrium isotherms, is defined as follows.[13]

For any given set $\{r_e, \tilde{T}, \tilde{T}_{\Sigma c}, \psi\}$, a solution θ_e of eq 3 or 4 is said to be (asymptotically) m-stable if there is a neighborhood of θ_e such that any θ inside this neighborhood approaches θ_e as time increases.

It follows from the definition that a very simple criterion for deciding whether any point on an equilibrium isotherm is m-stable is as follows:

θ_e is an m-stable equilibrium solution if and only if $\Delta\tilde{\mu}$ changes from negative to positive values when $\theta - \theta_e$ does so.

Indeed, referring to Figure 1, and keeping eq 59 in mind, one sees that, if the condition is satisfied, then any perturbation

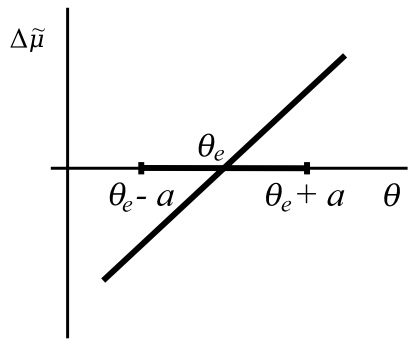

Figure 1. Figure used in defining *m*-stability in Section 2.2. If $\Delta\tilde{\mu}$ vs θ behaves as shown in the vicinity of θ_e, then θ_e is m-stable.

of θ_e that takes place during time $d\tilde{t} > 0$, and that brings θ in the interval $(\theta_e, \theta_e + a)$, gives rise to $\Delta\tilde{\mu} > 0$. It follows that $d\theta = -\Delta\tilde{\mu}\, d\tilde{t} < 0$, so that θ is drawn back to θ_e. A similar reasoning can be made for a perturbation that brings θ to the left of θ_e, with the same conclusion that θ is drawn back to θ_e. Necessity is also easily proven.

2.3. Analytical Equilibrium Isotherms and Their Stability. Analytical solutions of eq 4 are considered here.

DOI: 10.1021/acsomega.9b02956
ACS Omega 2020, 5, 430−447

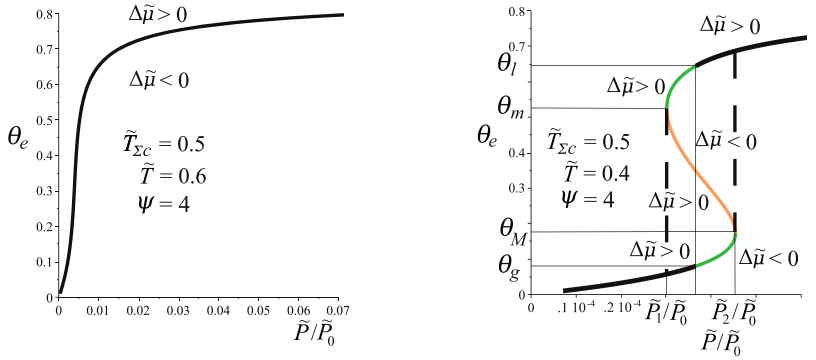

Figure 2. Plots of eq 6, for a supercritical (left) or subcritical (right) adsorbate for values of $\tilde{T}$, $\tilde{T}_{\Sigma c}$, and ψ, as indicated. The right plot uses the notations of Figure 14 for the subscripted θ's, as well as for the meanings of the colors. Concerning the vertical dashed lines in the right plot, see Section 2.3.

More precisely, one seeks to express θ_e as a known function of r_e or vice versa. Obviously, this is only possible if one knows how to invert either $\tilde{f}_\Sigma$ or $\tilde{f}_f$. No inverse of $\tilde{f}_\Sigma$, given by eq 46 (right), is known. Inverting $\tilde{f}_f$, however, may be possible as shown below. There are three acceptable approximations for the ambient fluid fugacity, and two of them are invertible: the ones obtained by assuming that the ambient fluid is ideal, either of type zero (zero volume particles) or of type 1 (nonzero volume particles). The relevant expressions for $\tilde{f}_f$ are given in eq 47 (right) and 48 (right). In fact, most analytical isotherms are expressions giving *pressure* as a function of coverage, see for example, Table I-1 in the book by Ross and Olivier.[14] This can easily be done in the present case by writing each invertible fugacity in terms of the corresponding pressure. Referring to the left and center equations of the set (36), it is easily seen that

$$\tilde{f}_f^{id0} = \tilde{P}^{id0}, \qquad \tilde{f}_f^{id1} = \tilde{P}^{id1} \exp\left(\frac{\tilde{P}^{id1}}{\tilde{T}}\right)$$

Assuming that the ambient gas can be approximated by an ideal gas of type 0, eq 4 gives the known expression

$$\tilde{P}^{id0} = \frac{\tilde{f}_\Sigma}{\tilde{K}_H} = \frac{\tilde{T}}{\tilde{K}_H} \frac{\theta_e}{1-\theta_e} \exp\left(\frac{\theta_e}{1-\theta_e} - \frac{27\theta_e}{\tau}\right) \tag{5}$$

Assuming that the ambient gas can be approximated by an ideal gas of type 1, eq 4 gives

$$\frac{\tilde{f}_\Sigma}{\tilde{K}_H \tilde{T}} = \frac{\tilde{P}^{id1}}{\tilde{T}} \exp\left(\frac{\tilde{P}^{id1}}{\tilde{T}}\right)$$

This equation is of the type $Z \exp Z = g$ and, g being positive, is equivalent to $Z = \mathrm{Wp}(g)$, where Wp is the principal part of the Lambert W-function.[15] One thus obtains

$$\tilde{P}^{id1} = \tilde{T}\,\mathrm{Wp}\left(\frac{\tilde{f}_\Sigma}{\tilde{K}_H \tilde{T}}\right), \qquad = \tilde{T}\,\mathrm{Wp}\left(\frac{1}{\tilde{K}_H} \frac{\theta_e}{1-\theta_e} \exp\left(\frac{\theta_e}{1-\theta_e} - \frac{27\theta_e}{\tau}\right)\right) \tag{6}$$

To the author's knowledge, this equation has not previously appeared in the adsorption literature. A plot of θ_e versus $\tilde{P}^{id\,0}$ is usually quite close to a plot of θ_e versus $\tilde{P}^{id\,1}$, except for ψ-values less than 1 and for θ_e-values close to 1.

One now turns to the restrictions mentioned in Section 2.1, so as to establish whether the expressions above are acceptable.

Plots of eq 6, say, show continuous curves, monotonic increasing when $\tilde{T} > \tilde{T}_{\Sigma c}$ (Figure 2, left-hand plot), but with a region of three-valuedness when $\tilde{T} < \tilde{T}_{\Sigma c}$ (Figure 2, right plot).[a]

The m-stability of the supercritical isotherm (left plot of Figure 2) is established as follows. Letting θ move on a vertical line, say upward from a low value, then $\theta - \theta_e$ and $\Delta\tilde{\mu}$ both go from negative to positive values when the isotherm is crossed. The necessary and sufficient condition stated in Section 2.2 is satisfied, so that the supercritical isotherm is m-stable. It is also physically stable (p-stable) because ambient gas and the adsorbate behave nearly ideally. One thus recovers the known result that the supercritical isotherms given by eq 5 are physically correct.

Turning to the subcritical case (right plot of Figure 2), one sees that the isotherm has three parts: a central part, whose states are p-unstable (orange line), connecting a lower to an upper part. The lower is here called the adsorption branch, and the upper is called the desorption branch. Each of these branches contains a set of p-stable states (black line) and a set of p-metastable states (green line). The m-stabilities of the three parts are established by the same argument as used in the supercritical case. One easily finds that the central part (orange line) consists of m-unstable states, so that there is no doubt in discarding these points that already are p-unstable. However, all points on the adsorption and desorption branches are, with the exception of one point for each branch, m-stable, regardless of the quality of their physical stability: the whole set of p-stable points and almost the whole set of p-metastable points are m-stable. The exception is, for each branch, the p-metastable point having a vertical tangent, that is, the point on the isotherm where $\theta = \theta_m$ (desorption branch) or $\theta = \theta_M$ (adsorption branch): indeed, repeating the m-stability argument, and letting θ move on a vertical tangent, then $\Delta\tilde{\mu}$ does not change sign when $\theta - \theta_{\substack{m \\ M}}$ does. The m-instability of these points is important in interpreting the region of two-valuedness as a hysteresis loop with the following boundaries: its upper and lower boundaries coincide with the desorption and adsorption branches over a pressure interval $[\tilde{P}_1, \tilde{P}_2]$. $\tilde{P}_2$ is the abscissa of the point on the adsorption branch whose ordinate is the left spinodal coverage, θ_M, whereas $\tilde{P}_1$ is the abscissa of the point on the desorption branch whose ordinate is the right spinodal coverage, θ_m. Note that the left and right boundaries of the hysteresis loop can only be the vertical lines

DOI: 10.1021/acsomega.9b02956
ACS Omega 2020, 5, 430−447

at $\tilde{P} = \tilde{P}_1$ and $\tilde{P} = \tilde{P}_2$ because $(\tilde{P}_1, \theta_m)$ and $(\tilde{P}_2, \theta_M)$ are the only m-unstable points on the desorption and the adsorption branches: the transition to a mathematically and physically stable state can only take place from $(\tilde{P}_2, \theta_M)$ during adsorption, and from $(\tilde{P}_1, \theta_m)$ during desorption. See Figure 2, right plot. Note also that the vertical boundaries of the hysteresis loop are not places of equilibrium, as these are in regions where $\Delta\tilde{\mu} \neq 0$. They are drawn as dashed lines in Figure 2 to emphasize this fact.

A further remark on the p-metastable states follows: by definition, a p-metastable adsorbate state will, if perturbed, transit to a p-stable state of lower energy. Referring to Figure 14 (right), such a transition brings the adsorbate from a point on one of the green lines to the reconstructed dash-dotted line at the same value of coverage. This implies that it is not possible to say whether an equilibrium state represented by a point situated on one of the green lines of Figure 2 (right plot) is in a two-phase or in a one-phase adsorbate state: the two states have the same coverage and also the same ambient pressure. The equality of pressures is approximative and is due to the assumptions that characterize M′, implying that changes in the adsorbate are not "visible" in the ambient gas. As a consequence, p-stable and p-metastable adsorbate states are treated in the same way in Section 2.5 below.

Thus, for equilibrium isotherms that can be obtained from analytical expressions, model M′ defines a subcritical equilibrium isotherm plotted against pressure as follows: it has an adsorption branch that spans all pressures up to a pressure $\tilde{P}_2$ at which the adsorbate is at its left spinodal coverage, θ_M. It has a desorption branch that spans pressures down to a pressure $\tilde{P}_1$ at which the adsorbate is at its right spinodal coverage θ_m. $\tilde{P}_1 < \tilde{P}_2$, hence, the interval $(\tilde{P}_1, \tilde{P}_2)$ defines the pressure range of the hysteresis loop. The vertical boundaries of the loop at pressures $\tilde{P}_1$ and $\tilde{P}_2$ do not consist of equilibrium points.

Sections 2.4 and 2.5 look at supercritical and at subcritical isotherms in cases where no analytical solution is available, that is, when $\tilde{\mu}_{f,red}$ is given by eq 49 (left).

2.4. Numerical Equilibrium Isotherms for Supercritical Adsorbates and Their Stability. Model M′ is now considered for the general case of numerically solving eq 3 for $\tilde{T} \geq \tilde{T}_{\Sigma c}$.

According to eq 56, the $\Delta\tilde{\mu}$ versus θ curve, at given r_e, $\tilde{T}$, $\tilde{T}_{\Sigma c}$, and ψ, is the $\tilde{\mu}_{\Sigma,red}$ versus θ curve with a vertical translation induced by $\tilde{\mu}_{f,red}(r_e, \tilde{T})$ and by $\psi(\tilde{T})$. The $\tilde{\mu}_{\Sigma,red}$ versus θ curve has the shape of the monotonically increasing curve shown in Figure 15 (right). One can immediately conclude that there will always be a solution (as the curve spans the vertical axis from $-\infty$ to $+\infty$), and that it is unique. Using mathematical stability, as defined in Section 2.2, together with the plots of $\Delta\tilde{\mu}$ versus θ, one concludes that $\theta_e(r_e)$ is m-stable in addition to being p-stable. For later reference, this equilibrium solution is written as

$$\theta_e(r_e, \tilde{T}, \tilde{T}_{\Sigma c}, \psi) = \text{unique solution of eq 3,} \quad (\tilde{T} \geq \tilde{T}_{\Sigma c}) \tag{7}$$

Its general shape is given in Figure 2 (left).

The interpretation of eq 3 as the intersection with the θ-axis of a vertically translated $\tilde{\mu}_{\Sigma,red}$ versus θ curve has some useful consequences concerning the general shape of an equilibrium supercritical isotherm, especially the location of its point of inflection.

Knowing the set $\{\tilde{T}, \tilde{T}_{\Sigma c}, \psi\}$, it is possible to roughly predict the position of the region where the isotherm is steepest, assuming that the parameters in the set above are such that the isotherm flattens out. This follows from the observation that the $\tilde{\mu}_{\Sigma,red}$ versus θ curve can be translated upward by an arbitrary amount by letting r_e go arbitrarily close to 0. Letting r_e increase from such a value, the $\tilde{\mu}_{\Sigma,red}$ versus θ curve is translated downward, and its intersection with the θ axis gives values of θ_e that increase, the fastest increase taking place when the inflection point of the $\tilde{\mu}_{\Sigma,red}$ versus θ curve is close to the θ-axis. This can only happen if ψ (the other quantity that is subtracted from $\tilde{\mu}_{\Sigma,red}$ in the expression of $\Delta\tilde{\mu}$) is large enough. It is then useful to define a function $\Psi_u(\tilde{T}, \tilde{T}_{\Sigma c})$ as follows: if $\psi = \Psi_u$, then the inflection point of the $\Delta\tilde{\mu}$ versus θ curve, at given $\tilde{T}$, $\tilde{T}_{\Sigma c}$, and at $r = r_g(\tilde{T})$, is on the θ-axis. The inflection point, easily found by equating to zero the second derivative of $\tilde{\mu}_{\Sigma,red}$ with respect to θ, occurs at $\theta = 1/3$, independently of $\tilde{T}$ and of $\tilde{T}_{\Sigma c}$, so that

$$\Psi_u(\tilde{T}, \tilde{T}_{\Sigma c}) = \tilde{\mu}_{\Sigma,red}(1/3, \tilde{T}, \tilde{T}_{\Sigma c}) - \tilde{\mu}_{f,red}(r_g(\tilde{T}), \tilde{T}) \tag{8}$$

See Figure 4 for the general behavior of Ψ_u. Note that Ψ_u does not depend on the values in the set $\mathcal{D}$.

Figure 3, shows how the shape of the equilibrium isotherm changes for values of ψ in the neighborhood of Ψ_u. Note that the tendency toward flattening occurs when $\psi > \Psi_u$.

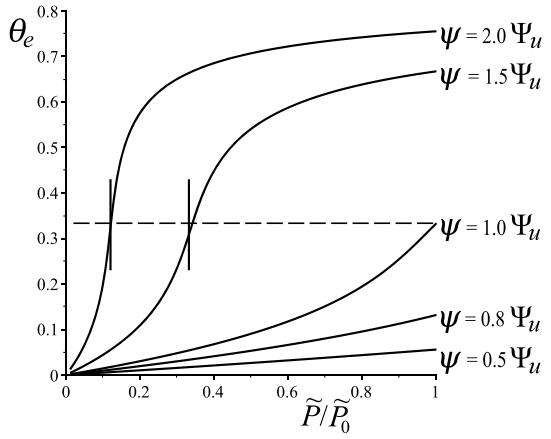

Figure 3. Equilibrium supercritical isotherms, θ_e vs $\tilde{P}/\tilde{P}_0$, where $\tilde{T}_{\Sigma c} = 0.5$ and $\tilde{T} = 0.6$. Curves originate from eq 7. The value of ψ is indicated for each curve ($\Psi_u = 1.2188$). The horizontal dashed line is at $\theta_e = 1/3$. Concerning the vertical segments, see the end of Section 2.4.

On an equilibrium isotherm plotted as θ_e versus r_e, one can find the approximate position of its point of inflection. It is the value of r_e, here denoted r_i, that corresponds to $\theta_e = 1/3$. According to eq 4, it is given by

$$\tilde{f}_f(r_i, \tilde{T}) = e^{-\psi/\tilde{T}} \tilde{f}_\Sigma(1/3, \tilde{T}, \tau) \tag{9}$$

One can obtain a good approximation for this r_i if one can assume that it is sufficiently close to 0 that $\tilde{f}_f \approx \tilde{T} r_i$ (see eq 47 (right)). Then, using eq 46 (right), one gets

$$r_i = \frac{e^{1/2 - 9/4\tau}}{2} e^{-\psi/\tilde{T}} = \frac{e^{1/2 - 9/4\tau}}{2\tilde{K}_H} \tag{10}$$

In Figure 3, the values of $\tilde{T} r_i/\tilde{P}_0$ given by this expression for $\psi = 1.5\Psi_u$ and $2.0\Psi_u$ are indicated by the vertical segments.

DOI: 10.1021/acsomega.9b02956
ACS Omega 2020, 5, 430−447

2.5. Numerical Equilibrium Isotherms for Subcritical Adsorbates and Their Stability. Returning to the interpretation of eq 3 as the intersection with the θ-axis of a vertically translated $\tilde{\mu}_{\Sigma,red}$ versus θ curve, one now assumes $\tilde{T} < \tilde{T}_{\Sigma c}$, so that the $\tilde{\mu}_{\Sigma,red}$ versus θ curve has a local maximum and a local minimum as shown in Figure 15 (right). There can now be one, two, or three values of θ_e, depending on the position of the $\Delta\tilde{\mu}$ versus θ curve in relation to the θ-axis. This position depends, in turn, on the values of $\tilde{\mu}_{f,red}$ and ψ.

The use of mathematical stability in this case leads to the following. If there is just one value of θ_e, then it occurs as the intersection with the θ-axis of that part of the translated $\tilde{\mu}_{\Sigma,red}$ versus θ curve that is either to the left of the local maximum or to the right of the local minimum and is therefore m-stable. If there are two distinct values of θ_e, then one of them is m-stable, the other (being the abscissa of the local maximum or minimum) is m-unstable and discarded. If there are three values of θ_e, then: (i) the smallest and largest are m-stable, whereas the middle one is m-unstable and discarded; (ii) the smallest is in the interval $(0, \theta_M)$, and the largest is in the interval $(\theta_m, 1)$.

For later reference, the m-stable equilibrium solutions are written

$$\theta_{ea}(r_e, \tilde{T}, \tilde{T}_{\Sigma c}, \psi) = \text{solution of eq 3 in } (0, \theta_M), \quad (\tilde{T} < \tilde{T}_{\Sigma c}) \tag{11}$$

$$\theta_{ed}(r_e, \tilde{T}, \tilde{T}_{\Sigma c}, \psi) = \text{solution of eq 3 in } (\theta_m, 1), \quad (\tilde{T} < \tilde{T}_{\Sigma c}) \tag{12}$$

Because $\theta_M < \theta_m$, there are two separate branches as in Section 2.3, an adsorption branch, θ_{ea}, and a desorption branch, θ_{ed}, creating a double-valuedness for certain pressures. As in the right plot of Figure 2, this is interpreted to mean that there is a hysteresis loop and a phase transition for the adsorbate.

The sizes of ψ and of r_g being important, one is led to define the following two functions of $\tilde{T}$ and $\tilde{T}_{\Sigma c}$

$$\Psi_m(\tilde{T}, \tilde{T}_{\Sigma c}) = \tilde{\mu}_{\Sigma,red}(\theta_m, \tilde{T}, \tilde{T}_{\Sigma c}) - \tilde{\mu}_{f,red}(r_g, \tilde{T}) \tag{13}$$

$$\Psi_M(\tilde{T}, \tilde{T}_{\Sigma c}) = \tilde{\mu}_{\Sigma,red}(\theta_M, \tilde{T}, \tilde{T}_{\Sigma c}) - \tilde{\mu}_{f,red}(r_g, \tilde{T}) \tag{14}$$

where θ_m and θ_M are as defined in Figures 14 and 15, and by eq 37. It is easily seen that $\Psi_m < \Psi_M$. Both functions depend on $\tilde{T}$ and $\tilde{T}_{\Sigma c}$ and not on the set $\mathcal{D}$. Figure 4 shows the behavior of Ψ_m, Ψ_M, and Ψ_u versus $\tilde{T}$ for $\tilde{T}_{\Sigma c} = 0.5$.

It is now clear that the shape of an isotherm critically depends on the value of ψ. To make a more detailed description, plots of $\Delta\tilde{\mu}(\theta,r,\tilde{T},\tilde{T}_{\Sigma c},\psi)$ versus θ are shown in the third row of Figure 5, where the parameters are chosen as follows: $\tilde{T} = 0.4$, $\tilde{T}_{\Sigma c} = 0.5$; r is given its maximum value, $r_g(\tilde{T})$, consistent with the assumption that the ambient fluid is a gas; finally, $\psi < \Psi_m$ (left-hand plot), $\Psi_m < \psi < \Psi_M$ (center plot), and $\psi > \Psi_M$ (right-hand plot). Obviously, the value of ψ determines the position of the curve relative to the θ-axis, given that $r = r_g$.

One can now draw θ_e versus r_e for the three ψ-cases given above by gradually reducing r_e from r_g to 0 and getting the corresponding value(s) of θ_e. Graphically, this means translating the curves shown in the third row vertically upward, and noting the values of θ_e at which the black lines cross the θ-axis: the intersection of the black line to the left gives θ_{ea}, whereas the black line to the right gives θ_{ed}. Numerically, by using eqs 11 and 12. Functions θ_{ea} and θ_{ed} plotted against r_e or, equivalently against the pressure, are shown as solid lines in the fourth row of Figure 5. It is graphically obvious that θ_{ed} does not exist for the case $0 < \psi < \Psi_m$, and that both θ_{ea} and θ_{ed} exist for larger ψ-values, albeit for a limited range for r or $\tilde{P}$ values. The dotted lines that connect the desorption and the adsorption branches are the isotherms given by eq 6. See, for comparison, the right plot in Figure 2, and note, in particular that $\tilde{P}(r_1,\tilde{T}) = \tilde{P}_1$ and that $\tilde{P}(r_2,\tilde{T}) = \tilde{P}_2$.

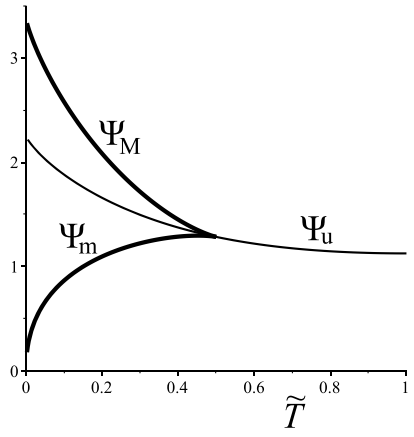

Figure 4. Special ψ's versus dimensionless temperature, $\tilde{T}$. The upper thick line is Ψ_M defined by eq 14, the lower thick line is Ψ_m defined by eq 13, and the thin line is Ψ_u, defined by eq 8. The first two are defined for $0 < \tilde{T} < \tilde{T}_{\Sigma c}$, whereas the last is defined for $\tilde{T} > 0$. All curves are drawn with $\tilde{T}_{\Sigma c} = 0.5$.

One sees that the adsorption branches, shown in the fourth row, only reach the value $r = r_2 < r_g$, if ψ is large enough that the local maximum of the $\Delta\tilde{\mu}$ versus θ curve is below the θ-axis when $r = r_g$, so that lifting the curve by reducing r brings the local maximum on the θ-axis when $r = r_2$: see the third column of the fourth row. Note also that, when this occurs, the adsorption branch stops being defined and that it seems to have a vertical tangent at $r = r_2$. Similar statements hold for the desorption branch.

The statements that the adsorption branch stops at r_2, whereas the desorption branch stops at r_1, both with vertical tangents, are correct because an equilibrium isotherm is a curve satisfying $\tilde{\mu}_{\Sigma,red}(\theta_e,\tilde{T},\tilde{T}_{\Sigma c}) - \tilde{\mu}_{f,red}(r_e,\tilde{T}) - \psi = 0$, whose tangents are given by

$$\frac{d\theta_e}{dr_e} = \frac{\partial\tilde{\mu}_{f,red}/\partial r_e}{\partial\tilde{\mu}_{\Sigma,red}/\partial\theta_e}$$

Thus, the local extrema of the $\tilde{\mu}_{\Sigma,red}$ versus θ curve produce vertical tangents on the isotherms, and there is agreement with the case of the analytical equilibrium isotherms, Section 2.3. The agreement goes, in fact, deeper because it is possible to repeat the stability analysis of Section 2.3 for the isotherms, and also for the points with vertical tangents, with the same conclusions.

It is now possible to interpret the multivaluedness in the equilibrium isotherms, by introducing a hysteresis loop.

Referring first to the plots of the third column, fourth and fifth rows of Figure 5, one interprets the two-valuedness of coverage as in Section 2.3: there is an adsorption curve abcd$\beta\alpha$, and a desorption curve $\alpha\beta\gamma\delta$ba. As pointed out in

DOI: 10.1021/acsomega.9b02956
ACS Omega 2020, 5, 430−447

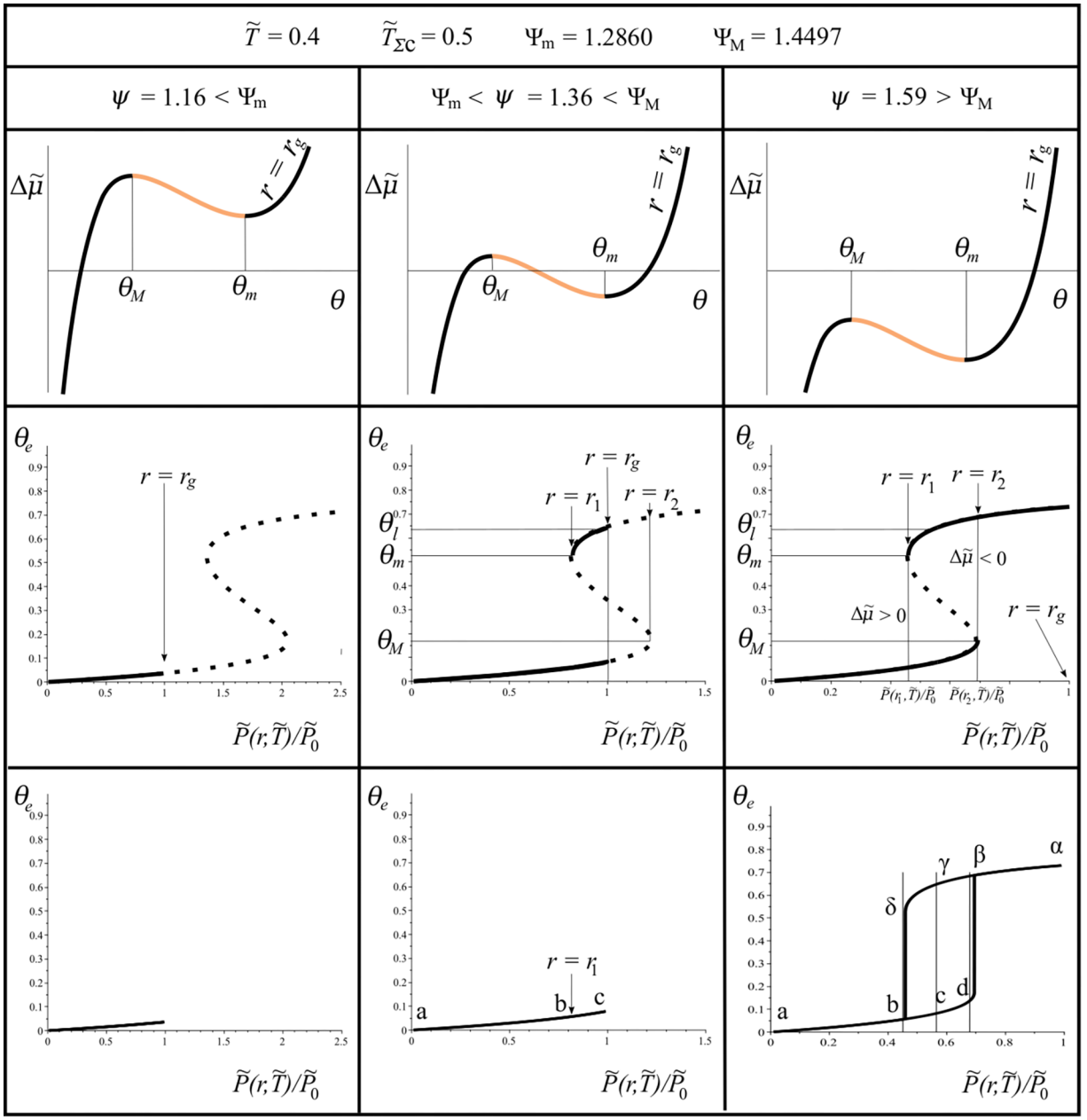

Figure 5. Illustrating the numerical calculation of equilibrium isotherms for subcritical temperatures. All plots are done with $\tilde{T} = 0.4$ and $\tilde{T}_{\Sigma c} = 0.5$. The values of ψ are, column-wise: $\psi < \Psi_m$ (left), $\Psi_m < \psi < \Psi_M$ (center), and $\psi > \Psi_M$ (right). For the plots of the third row, it is reminded that $\Delta\tilde{\mu} = \tilde{\mu}_{\Sigma,\mathrm{red}}(\theta, \tilde{T}, \tilde{T}_{\Sigma c}) - \tilde{\mu}_{\mathrm{f,red}}(r, \tilde{T}) - \psi(\tilde{T}, \mathcal{D})$. See text in Section 2.5, after eq 14.

Section 2.3, no solution of eq 11 or of eq 12 will be situated on one of the vertical boundaries of the hysteresis loop bcd$\beta\gamma\delta$.

The ambient densities r_1 and r_2, identifying the left and right boundaries of the hysteresis loop (see the fourth row in Figure 5) are functions of $\tilde{T}$, $\tilde{T}_{\Sigma c}$, and ψ, easily calculable by the following expressions

$$r_1 = x \in (0, r_g) \text{ such that } \Delta\mu(\theta_m, x, \tilde{T}, \tilde{T}_{\Sigma c}, \psi) = 0, \quad (\psi > \Psi_m) \tag{15}$$

$$r_2 = x \in (0, r_g) \text{ such that } \Delta\mu(\theta_M, x, \tilde{T}, \tilde{T}_{\Sigma c}, \psi) = 0, \quad (\psi > \Psi_M) \tag{16}$$

Turning now to the plots of the second column, fourth and fifth rows of Figure 5, it is seen that the upper solid line of the plot in the fourth row must be discarded as a possible equilibrium isotherm, at least if one assumes that desorption occurs after adsorption, because adsorption stops before the mathematically unstable point (where $\theta = \theta_M$) is reached, and the adsorbate has not transited to the desorption branch. Adsorption occurs along abc, stops at c because of the $\tilde{P} < \tilde{P}_0$ condition, and then desorption follows the adsorption branch but in the reverse direction, that is, along cba.

An important conclusion follows: there are two main classes for the values of ψ: the class $\psi \leq \Psi_M$ in which the isotherms show low coverage and are structureless (fifth row, left-hand and center plots in Figure 5) and the class $\psi > \Psi_M$ in which the

DOI: 10.1021/acsomega.9b02956
ACS Omega 2020, 5, 430−447

isotherms show an adsorbate phase transition and a hysteresis loop (fifth row, right-hand plot).

When $\psi > \Psi_M$, it is of some interest to predict the approximate pressure of the center of the loop, and also the pressures of its left and right vertical boundaries. The pressure in the approximate middle of the loop is $\tilde{P}(r_i,\tilde{T})$ where r_i is the previously found density at which the ambient chemical potential has an inflection point, see eq 10. The pressures approximating the left and right vertical boundaries are $\tilde{P}(r_1,\tilde{T})$ and $\tilde{P}(r_2,\tilde{T})$ where approximate expressions can be found for r_1 and r_2 in a manner similar to the one that led to eq 10. Equations 15, and 16 are equivalent to

$$\tilde{f}_\Sigma(\theta_m, \tilde{T}, \tau) = \tilde{K}_H \tilde{f}_f(r_1, \tilde{T}),$$
$$\tilde{f}_\Sigma(\theta_M, \tilde{T}, \tau) = \tilde{K}_H \tilde{f}_f(r_2, \tilde{T})$$

and assuming that r_1 and r_2 are small, one finds

$$r_1(\tilde{T}, \tilde{T}_{\Sigma c}, \psi) = E_m(\tau)\, e^{-\psi/\tilde{T}} = \frac{E_m(\tau)}{\tilde{K}_H},$$
$$r_2(\tilde{T}, \tilde{T}_{\Sigma c}, \psi) = E_M(\psi)\, e^{-\psi/\tilde{T}} = \frac{E_M(\tau)}{\tilde{K}_H} \quad (17)$$

where

$$E_m(\tau) = \frac{\tilde{f}_\Sigma(\theta_m, \tilde{T}, \tau)}{\tilde{T}} = \frac{\theta_m}{1-\theta_m}\exp\left(\frac{\theta_m}{1-\theta_m} - \frac{27}{4}\frac{\theta_m}{\tau}\right) \quad (18)$$

(E_M being obtained from above by substituting M to m) and where θ_m and θ_M are the functions of τ given by eq 37.

In the same approximation for which the above expressions are valid (low values of r), one can write the width of the hysteresis loop, in units of pressure, as $w = 8P_c\tilde{T}(r_2 - r_1)$ (see eq 33, right), that is

$$w = 8P_c\tilde{T}[E_M(\tau) - E_m(\tau)]\, e^{-\psi/\tilde{T}} = \frac{8P_c\tilde{T}[E_M(\tau) - E_m(\tau)]}{\tilde{K}_H} \quad (19)$$

$E_M - E_m$ versus τ is shown in Figure 6. The three pressures $\tilde{P}(r_i,\tilde{T})$, $\tilde{P}(r_1,\tilde{T})$, and $\tilde{P}(r_2,\tilde{T})$ are indicated by vertical lines on the plot of the fifth row and third column in Figure 5.

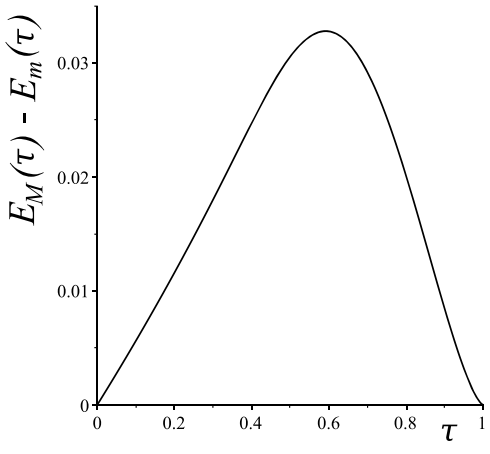

Figure 6. For $\tau = \tilde{T}/\tilde{T}_{\Sigma c} < 1$, the width of the hysteresis loop is proportional to $E_M - E_m$ (see eq 19), a function of τ that vanishes at $\tau = 0$ and $\tau = 1$. Its maximum, 0.03281 is attained when $\tau = 0.5917$.

3. RESULT AND DISCUSSION 2: THEORY OF TIME-DEPENDENT ISOTHERMS

Time-dependent solutions of eq 59 are now considered, that simulate the thought experiment described in the next paragraph below, leading to a description of dynamical isotherms, and to their behavior in relation to equilibrium isotherms and to hysteresis loops. Two subcases are considered: the supercritical and the subcritical adsorbate. It is believed that the actual values of $\tilde{T}$ and $\tilde{T}_{\Sigma c}$ are of secondary importance as compared to their relative sizes. $\tilde{T}_{\Sigma c} = 0.5$ has been used repeatedly above, and is also used in what follows, whereas $\tilde{T} = 0.6$ and $\tilde{T} = 0.4$ are used for the two cases.

The thought-experiment considered is as follows. An amount of mesoporous or macroporous medium is placed in a container filled with a one-component gas at low pressure P and at uniform constant temperature T, which is less that the critical temperature. After the gas in the pores has settled into a state of zero velocity and uniform pressure P_i, which is less than the saturation pressure P_0, the pressure in the gas is slowly increased to a pressure $P_f \le P_0$, then slowly decreased back to P_i. Recordings of the amounts adsorbed, and of the corresponding ambient densities or pressures are assumed to occur continuously. The duration of the cycle $P_i \to P_f \to P_i$ is assumed to be large enough for the ambient density to remain nearly uniform, and for the ambient velocity to be nearly zero, in the macroporous medium at all times. (See the description of model M′ in the Introduction.)

The cycle of applied pressure forces the ambient density to follow a similar cycle. In M′, $r(\tilde{t})$ is needed as extra input to solve eq 59. Mathematically, one can introduce a function $\tilde{P}(\tilde{t})$ and find the resulting $r(\tilde{t})$ by solving the equation of state. A simplification is described in what follows, that avoids time-consuming calculations by starting directly with a function $r(\tilde{t})$ that goes through a cycle, starting from a low-value r_e, increasing to a high-value $r_t \le r_g$, then decreasing back to r_e. Such a function is shown in Figure 7, where the increasing and

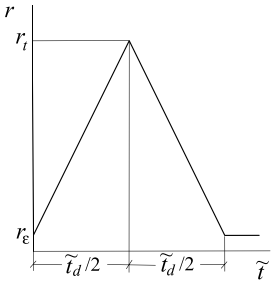

Figure 7. Function $r(\mathcal{P}; \tilde{t})$, where $\mathcal{P}$ is the set of three parameters $\{r_e, r_t, \tilde{t}_d\}$. The function simulates a compression−decompression cycle.

decreasing parts are linear. The minimum r_e is introduced so as to avoid the singularity of the chemical potential at $r = 0$, and a value $r_e = r_t/10^3$ is in general sufficient. The figure defines $r(\mathcal{P}; \tilde{t})$, where $\mathcal{P}$ is the set of three parameters $\{r_e, r_t, \tilde{t}_d\}$. The time parameter, $\tilde{t}_d$ will be called the cycle duration.

Equation 59 is solved[b] with an initial condition, $\theta(0) = r(\mathcal{P}; 0)\exp(\psi/\tilde{T})$. Concerning the arguments of $\Delta\tilde{\mu}$, $r(\mathcal{P}; \tilde{t})$ is substituted to r and, as already mentioned, $\tilde{T}_{\Sigma c} = 0.5$ and two values are considered for $\tilde{T}$, that is 0.4 and 0.6. The central purpose of the calculations is to determine the influence of the values of ψ and of the cycle duration $\tilde{t}_d$ on the shapes of the time-dependent isotherms.

DOI: 10.1021/acsomega.9b02956
ACS Omega 2020, 5, 430−447

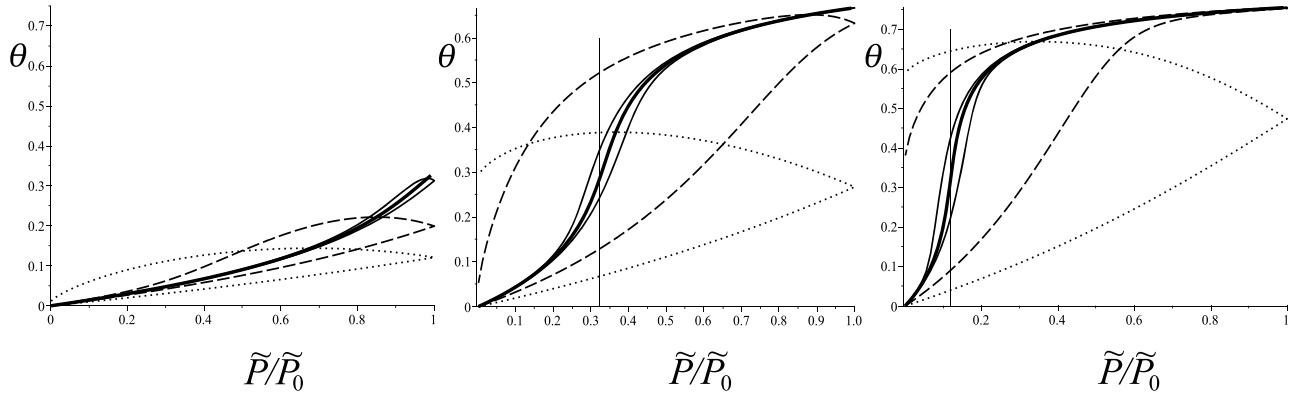

Figure 8. Isotherms for a supercritical adsorbate: $\tilde{T}_{\Sigma c} = 0.5$, $\tilde{T} = 0.6$. The values of ψ are, from the left to the right plot, equal to $\Psi_u = 1.22$, $1.5\Psi_u = 1.83$, and $2.0\Psi_u = 2.44$. The thick solid line is the equilibrium isotherm in each plot. For all plots, the values of the loop duration $\tilde{t}_d$ are: 1 for the dotted lines, 5 for the dashed lines, and 100 for the solid lines. The vertical thin lines are at $P(r_i, \tilde{T})$.

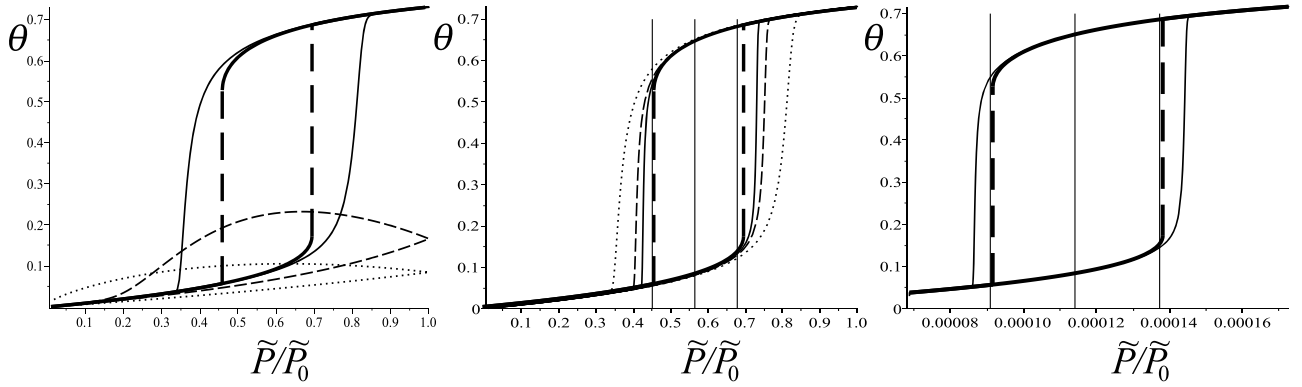

Figure 9. Isotherms for a subcritical adsorbate. For all three plots, $\tilde{T}_{\Sigma c} = 0.5$, $\tilde{T} = 0.4$, the thick solid lines are the equilibrium isotherms, and the thick dashed lines are the hysteresis boundaries. Left plot: $\psi = 1.1\Psi_M = 1.595$; dynamic isotherms calculated with $r_\epsilon = 0.01r_g$, $r_t = r_g$, $\tilde{t}_d = 1$ (thin dotted), 5 (thin dashed), 100 (thin solid). Center plot: $\psi = 1.1\Psi_M = 1.595$; $r_\epsilon = 0.01r_g$, $r_t = r_g$, $\tilde{t}_d = 100$ (thin dotted), 300 (thin dashed), 600 (thin solid). Right plot: $\psi = 5$; dynamic isotherm calculated with $r_\epsilon = 0.75r_1$, $r_t = 1.25r_2$, $\tilde{t}_d = 600$ (thin solid). In the center and right plots, the vertical thin lines are placed at $r = r_1, r_i, r_2$.

The supercritical case is examined first, and $\tilde{T} = 0.6$ is used. Figure 8 shows the results obtained as three plots, with four curves in each plot, and increasing values of ψ from left to right (based on the case of the equilibrium isotherms of Section 2.4). In each plot, the thick-lined curve is the equilibrium isotherm, and the other curves are dynamic isotherms with increasing cycle times, $\tilde{t}_d$ as indicated in the caption. The vertical thin lines are at the approximate positions of the inflection points of the equilibrium isotherms, given by eq 10. The most noticeable feature is exhibited by the dotted-line isotherms (short cycle duration), where adsorption increases long after the start of decompression. Also remarkable is the tendency of the isotherms to exhibit loops that resemble hysteresis loops found in magnetism, but that shrink when the cycle duration increases. This type of hysteresis was apparently first observed in piezoelectric measurements in 2003 and denoted then as rate-dependent hysteresis.[16]

Both features above are experimentally observed in adsorption, as shown in the review article by Wang et al.[9] For further discussion, see Section 4.

The subcritical case is now examined, and $\tilde{T} = 0.4$ is used, with $\tilde{T}_{\Sigma c} = 0.5$.

According to the conclusion drawn in Section 2.5, one can concentrate on cases where the equilibrium isotherms show phase transition and hysteresis, that is, the cases $\psi > \Psi_M$. The three plots in Figure 9 show equilibrium isotherms, vertical hysteresis boundaries, and dynamic isotherms resulting from various cycle durations, as indicated in the caption.

The dynamical isotherms in the left plot are calculated with the same cycle durations, $\tilde{t}_d$, used for the dynamical isotherms in Figure 8. They show, for small cycle durations, the same increase in adsorption even after the start of decompression. The center plot shows the tendency of the dynamical isotherms to approach the equilibrium isotherms when the cycle duration increases. In particular, the left and right boundaries of the hysteresis loop seem to attract the parts of the time-dependent isotherms that join low to high (or, for decompression, high to low) density adsorbate. However, the vertical hysteresis boundaries are not places of equilibrium, and the reason for the behavior of the time-dependent isotherms is that they are forced toward a vertical direction by being attracted to the parts of the upper and lower boundaries that rapidly curve from the near horizontal to the vertical.

The right plot, with $\psi = 5$, simulates conditions of high adsorption (see Figure 16). The notable fact here is that the phase transition and accompanying hysteresis loop happen at very low pressures, the width of the loop also being quite small. The center and right plots show that the placement and width of the loop are well described by r_i, r_1, and r_2, given by eqs 10 and 17.

DOI: 10.1021/acsomega.9b02956
ACS Omega 2020, 5, 430−447

4. RESULT AND DISCUSSION 3: REINTERPRETING THE SORPTION OF CO_2 AND CH_4 ON COAL

A number of publications (Zhao et al.[6] and refs 15−28 given there) report experiments of methane and carbon dioxide sorption, showing isotherms with hysteresis loops at temperatures where capillary condensation cannot explain the hysteresis.[6,9] In fact, these isotherms have loops that bear a strong resemblance to the one presented in Section 3, especially in Figure 8. One of these experiments is examined below in the framework of model M′.

The experiment in question is the one reported by Jessen et al.[7] It is here interpreted in a way that differs from the one given by the authors. Shortly stated, the authors fit one static isotherm to the adsorption data and another to the desorption data (both are Langmuir isotherms), thus obtaining two separate values for the Henry adsorption constant, one for adsorption and one for desorption. In model M′, however, it is possible to fit just one time-dependent isotherm to the set of data consisting of adsorption and desorption, and thus obtain a unique Henry constant. More precisely, M′ has two internal parameters, $\tilde{T}_{\Sigma c}$ and ψ. However, fitting an isotherm to the data requires, as shown below, the introduction of three additional parameters. The least squares principle is applied, whereby the best values of the parameters are the ones that minimize the sum of the squared differences between the measured and calculated values.

The raw data reported by Jessen et al.[7] concerning the adsorption−desorption at T_{exp} = 295.15 K of CO_2 by Wyoming coal, are shown plotted in Figure 10. Points are

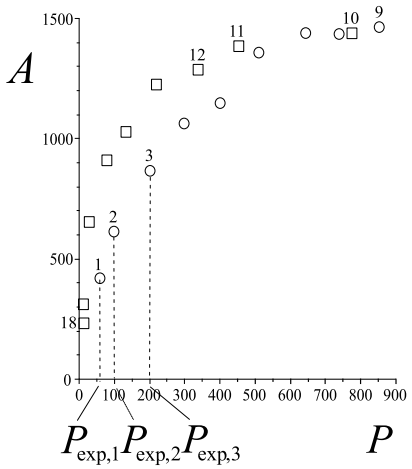

Figure 10. Adsorption (circles) and desorption (squares) of CO_2 by Wyoming coal at 295.15 K, as reported by Jessen et al.[7] The horizontal axis gives pressure in PSI. The vertical axis gives the amounts adsorbed, A, in SCF per ton of coal. For the numbering of the points, see the text.

numbered in increasing order for increasing (adsorption), and then decreasing (desorption) coverage. The coordinates of point i are denoted $(P_{exp,i}, A_{exp,i})$ where, for the adsorption points, i = 1, ..., N_a and for the desorption points, $i = N_a + 1$, ..., $N_a + N_d$, and $N_a = N_d = 9$. The amounts adsorbed are given in SCF per ton of coal.

According to the NIST database, the critical temperature and pressure for CO_2 are

$$T_{fc} = 304.2 \text{ K}, \qquad P_c = 7.38 \times 10^6 \text{ Pa} = 0.1070 \times 10^4 \text{ PSI} \tag{20}$$

The dimensionless temperature attached to the raw data of Figure 10 is thus $\tilde{T}_{exp} = T_{exp}/T_{fc} = 295.2/304.2 = 0.9704$.

The ambient CO_2 is thus slightly subcritical. Assuming an adsorbate critical temperature of about a half or less of the above T_{fc}, one concludes that the adsorbate is supercritical. According to model M′, if hysteresis is observed, it must be of one of the types drawn with a thin dashed or thin solid line on the right-hand plot in Figure 8. In other words, it can only be a rate-dependent hysteretic isotherm with a large value of t_r so that its shrinking to the unique curve representing the equilibrium isotherm is difficult to observe.

The experiment[7] is described as follows. Adsorption is driven by a series of compressions and relaxations, starting from an initial low pressure $P_{exp,1}$ and leading to a maximum pressure $P_{exp,9}$, which is less than saturation pressure (about 950 PSI at 295.15 K); desorption then follows, as a series of decompressions and relaxations leading back to a low pressure approximately equal to $P_{exp,18}$. The compression and decompression times are not given explicitly, but it is indicated that relaxation times are of at least 24 h.

In the framework of model M′, a simplified simulation of the experiment consists of solving eq 59, with a function $r(\tilde{t})$ that is not the simple compression−decompression cycle of Figure 7 but a cycle that includes a series of compressions and relaxations followed by a series of decompressions and relaxations, as shown in Figure 11. One then obtains

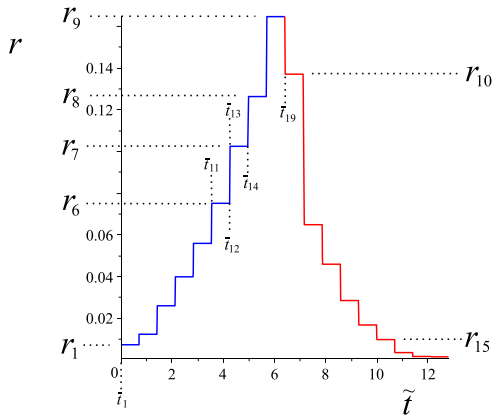

Figure 11. Function $r(\tilde{t})$ that simulates a series of compressions (the nearly vertical segments) and relaxations (the horizontal segments) followed by a series of decompressions and relaxations that lead to the measurement of the amounts of CO_2 adsorbed in the experiment by Jessen et al.[7] (their Figure 2). See the text in Section 4 for the construction of this function.

theoretical coverage θ, as a dimensionless number between 0 and 1, in terms of dimensionless time $\tilde{t}$. Parametric plots of θ versus r, with parameter $\tilde{t}$, can then be obtained. Recordings of theoretical coverage and ambient density are made immediately after compression (in adsorption) or decompression (in desorption), with the purpose of comparing them to the experimental points $(P_{exp,i}, A_{exp,i})$. Two subsidiary problems must obviously be solved: the first one is the same as mentioned in the third paragraph of Section 3, of going from pressure to density and back, and is solved by creating an array, $r_{exp,i}$, $(i = 1, ..., N_a + N_d)$, with elements satisfying $\tilde{P}(r_{exp,i}, \tilde{T}_{exp}) =$

DOI: 10.1021/acsomega.9b02956
ACS Omega 2020, 5, 430−447

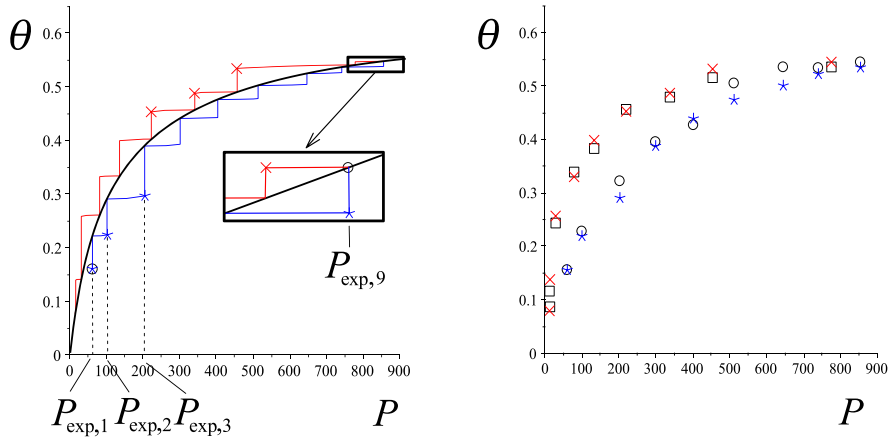

Figure 12. Interpretation of the experimental data shown in Figure 10. In both plots, the vertical axis gives dimensionless coverage; the horizontal axis gives ambient pressure in PSI. Left-hand plot: The smooth black curve is the theoretical equilibrium isotherm given by eq 7. The blue and red sawtooth curves, joined as shown in the inset, constitute the solution of eqs 23 and 24, the two colors referring to the colors in Figure 11. Asterisks and crosses indicate values to be compared to the measurements, see the right-hand plot. Right-hand plot: Circles and squares are the experimental data of Figure 10 for adsorption (circles) and desorption (squares) of CO_2 by Wyoming coal at 295.15 K.[7] Blue asterisks (adsorption) and red crosses (desorption) result from model calculations as indicated by the left-hand plot.

$\tilde{P}_{\mathrm{exp},i}$. The second is writing the experimental adsorptions $A_{\mathrm{exp},i}$ as dimensionless numbers $\theta_{\mathrm{exp},i}$ between 0 and 1. To solve this second problem, one introduces a constant C, defined as

$$\theta_{\mathrm{exp},i} = A_{\mathrm{exp},i}/C, \qquad (i = 1, ..., N_a + N_d) \tag{21}$$

For the determination of C, see item 3 in the algorithm below.

The simulation consists of several parts that are now described in more detail.

The first part is the construction of the function $r(\tilde{t})$ shown in Figure 11. It is done as follows.

It is assumed that a recording of $(P_{\mathrm{exp},i}, A_{\mathrm{exp},i})$ for some value of i is followed by a relaxation time that is large enough for the adsorbate coverage to reach its equilibrium value. Relaxation is followed by a compression (or a decompression) that brings pressure $P_{\mathrm{exp},i}$ to $P_{\mathrm{exp},i+1}$ (equivalently, $r_{\mathrm{exp},i}$ to $r_{\mathrm{exp},i+1}$) and to the recording of $A_{\mathrm{exp},i+1}$.

To minimize the number of parameters to be determined, it is assumed that the same relaxation time is used for all i, so that one relaxation time, $\mathcal{R}$, is introduced as a parameter to determine. Note, incidentally, that in theory, it takes infinite time to reach equilibrium so that $\mathcal{R}$ must be such that equilibrium is reached within a certain acceptable tolerance. See item 4 in the algorithm below.

Another parameter to determine is introduced: a time variable, C, used to quantize the rate of compression/decompression. Let C be the estimated time that is necessary to carry out the compression of the ambient gas from the lowest pressure, $P_{\mathrm{exp},1}$, to the highest adsorption pressure, $P_{\mathrm{exp},9}$, at a constant rate. Then, the rate of compression can be obtained as

$$v = (r_{\mathrm{exp},N_a} - r_{\mathrm{exp},1})/C \tag{22}$$

and the assumption is made that this rate is used to compress or decompress from any density to the next.

An array $\bar{t}_i$ is then constructed, where the first value, $\bar{t}_1$, is taken as the origin, assumed to be the time of the first data registration (labeled 1 in Figure 10); $\bar{t}_2$ is then the time at the end of the first relaxation. Then, $\bar{t}_k$, where $k = 3, ..., 18$ are the successive times at the ends of the compressions and relaxations leading to the last adsorbed value (labeled 9 in Figure 10)

$$\bar{t}_1 = 0,$$
$$\bar{t}_2 = \mathcal{R},$$
$$\bar{t}_{2n-1} = \bar{t}_{2n-2} + (r_{\mathrm{exp},n} - r_{\mathrm{exp},n-1})/v, \qquad (n = 2, ..., N_a),$$
$$\bar{t}_{2n} = \bar{t}_{2n-1} + \mathcal{R}, \qquad (n = 2, ..., N_a)$$

Times $\bar{t}_k$ where k runs from 11 to 14 are shown in Figure 11. Also shown is the time of the first desorption, $\bar{t}_{19}$, at the end of the first decompression. The last registered desorption (labeled 18 in Figure 10) is at $\bar{t}_{36}$

$$\bar{t}_{2N_a+2n-1} = \bar{t}_{2N_a+2n-2} + (r_{\mathrm{exp},N_a+n-1} - r_{\mathrm{exp},N_a+n})/v, \qquad (n = 1, ..., N_d),$$
$$\bar{t}_{2N_a+2n} = \bar{t}_{2N_a+2n-1} + \mathcal{R}, \qquad (n = 1, ..., N_d)$$

It is then useful to construct an array $\bar{r}$

$$\bar{r}_{2n-1} = r_n, \qquad (n = 1, ..., N_a + N_d),$$
$$\bar{r}_{2n} = r_n, \qquad (n = 1, ..., N_a + N_d)$$

so that the function $r(\tilde{t})$ of Figure 11 is the function that joins point $(\bar{t}_i, \bar{r}_i)$ to point $(\bar{t}_{i+1}, \bar{r}_{i+1})$ by a straight line, for $i = 1, ..., 2N_a + 2N_d - 1$.

According to the description given above of the simplified simulation of the experiment, the amounts adsorbed are recorded after compression (for adsorption) or after decompression (for desorption), that is, at times $\bar{t}_{2k-1}$ with $k = 1, ..., N_a + N_d$.

The second important part of the simulation is to find a solution of eq 59, where $r(\tilde{t})$ is the function shown in Figure 11. It is advantageous for accuracy to find the solution of eq 59 as a succession of solutions, where the different rectilinear parts of function $r(\tilde{t})$ are considered in turn. For each of the $2N_a + 2N_b - 1$ rectilinear parts, one thus defines a time variable, τ_n and a linear density function, ρ_n of τ_n, as follows

DOI: 10.1021/acsomega.9b02956
ACS Omega 2020, 5, 430−447

$$\tau_n = \frac{\tilde{t} - \bar{t}_n}{\bar{t}_{n+1} - \bar{t}_n},$$

$$\rho_n = (1 - \tau_n)\bar{r}_n + \tau_n \bar{r}_{n+1}$$

For each rectilinear part, a coverage, $\theta_n(\tau_n)$ is then defined iteratively as the solution of eq 59, rewritten in terms of the new quantities just introduced

$$\frac{d\theta_n}{d\tau_n} = -(\bar{t}_{n+1} - \bar{t}_n)\Delta\tilde{\mu}(\theta_n, \rho_n(\tau_n), \tilde{T}, \tilde{T}_{\Sigma c}, \psi) \quad (23)$$

$$\theta_n(0) = \theta_{n-1}(1) \quad (24)$$

This is done for $n = 1, ..., 2N_a + 2N_d - 1$, where, for $n = 1$, one defines $\theta_1(0) = \theta_{exp,1}$. This last is not an extra assumption because one can replace $\theta_{exp,1}$ by any other value in its vicinity, if one, simultaneously, agrees not to include the first deviation when minimizing the sum of the squared deviations (see item 5 in the algorithm below).

The final part of the simulation consists of finding the solution of eqs 23 and 24 that best fits the data. It involves the determination of the following set of parameters

$$\{\mathcal{R}, C, C, \tilde{T}_{\Sigma c}, \psi\}$$

in a way that minimizes the averaged sum of the squared deviations $(\theta(\bar{t}_{2n-1}) - \theta_{exp,n})^2$. This is done by the following algorithm.

1 Values are chosen for $\tilde{T}_{\Sigma c}$ and ψ, say 0.3 and 4, respectively.
2 Using eq 7, the equilibrium isotherm $\theta_e(r_e, \tilde{T}_{exp}, \tilde{T}_{\Sigma c}, \psi)$ is drawn. See the smooth curve in black in the left-hand plot in Figure 12.
3 The value of C (see eq 21) is calculated, that gives $\theta_e(r_{exp,9}, \tilde{T}_{exp}, \tilde{T}_{\Sigma c}, \psi) = A_{exp,9}/C$, and the data are replotted with ordinates $\theta_{expi} = A_{expi}/C$.
4 Values are chosen for $\mathcal{R}$ and C, say 1 and 0.1, and eqs 23 and 24 are solved for all n, as indicated. The value chosen for $\mathcal{R}$ is increased if relaxation, at any experimental point, ends before the equilibrium isotherm is reached (seen graphically as two lines touching, see the left-hand plot of Figure 12.), and the solutions are recalculated. The isotherm is plotted as a blue sawtoothed curve for adsorption, a red sawtoothed curve for desorption: see the left-hand plot on Figure 12. The coverage calculated by the model at the end of each compression is plotted as an asterisk, and the value calculated at the end of each decompression is plotted as a diagonal cross. (Not all asterisks and crosses are shown in the left-hand plot of Figure 12.)
5 The averaged sum of the squared deviations

$$D2 = \frac{1}{17}\left[\sum_{i=2}^{9}(\theta^*(r_{expi}) - \theta_{expi})^2 + \sum_{i=10}^{18}(\theta^\times(r_{expi}) - \theta_{expi})^2\right]^{1/2}$$

is calculated.

6 The values of the parameters are those that minimize $D2$.

Comments: (i) The value of C determined at the third step above has been taken as the final one with the justification that the experimental point number 9 is on the flat portion of the isotherm and therefore very close to the equilibrium isotherm. (ii) The value of $\mathcal{R}$, determined at the fourth step, need not be increased: any larger value will serve the same purpose because reducing the distance to the equilibrium isotherm below a certain small value has no interest. (iii) The value of C turns out to have little influence on the final result: C must be small compared to $\mathcal{R}$, and small values (0.1, say) give almost horizontal compression or decompression isotherm segments: a smaller value (0.01, say) might be unrealistic (depending on the value of t_r) without noticeably changing the shape of the isotherm segments.

The sawtoothed curves of the left-hand plot of Figure 12 are joined at $r_{exp,9}$ as shown by the inset, and can thus be seen as just one isotherm, "anchored" to the experimental points at the last adsorption measurement.

The minimum value of $D2$ is 0.00512, and is obtained with $\mathcal{R} = 0.7$, $C = 0.1$, and

$$\tilde{T}_{\Sigma c} = 0.000,$$

$$\psi = 3.83$$

The right-hand plot of Figure 12 shows theoretical coverage (asterisks and crosses) at pressure values where experimental coverage is given (circles and squares).

Comments: (i) The smallness of $\tilde{T}_{\Sigma c}$ indicates that an adsorbate of CO_2 on coal acts like an ideal gas of finite volume molecules. (ii) Model M′, used as described in this section, predicts unique values for $\tilde{T}_{\Sigma c}$ and ψ. In Jessen et al.[7] (see their Table 2 and Figure 2), adsorption and desorption are assumed to evolve along different equilibrium isotherms, so that two values of ψ result: 3.66 for adsorption and 4.73 for desorption.

Turning now to the data reported[7] concerning the adsorption−desorption at 295.15 K of CH_4 by Wyoming coal, one notes first that, according to the NIST database, the critical temperature for CH_4 is $T_{fc} = 190.6$ K, so that the ambient CH_4 is supercritical. The adsorbate critical temperature being most likely less than the above T_{fc}, the adsorbate is also supercritical. The experiment is then inside the framework of M′ because a phase transition for the ambient fluid is excluded, and uniformity of density can be assumed. (See the description of model M′ in the Introduction.) The situation is thus similar to that of the CO_2 experiment just gone through, that is, that of a rate-dependent hysteresis isotherm. Following the same procedure, one finds a minimum value of $D2$ equal to 0.0067, obtained with $\mathcal{R} = 0.7$, $C = 0.1$, and

$$\tilde{T}_{\Sigma c} = 0.3,$$

$$\psi = 5.8$$

Figure 13 shows experimental coverage (circles and squares) and theoretical coverage (asterisks and crosses) calculated at the same pressures. Using data from Table 2,[7] one finds that the two Langmuir curves that fit the adsorption and desorption CH_4 curves of Figure 2[7] yield two values for ψ: 4.61 for adsorption and 8.92 for desorption.

5. BACKGROUND MATERIAL

Material given here includes the explicit calculation of the thermodynamic functions of the ambient and adsorbed fluids, that is, pressure and spreading pressure (Section 5.1) and chemical potentials and fugacities (Section 5.2); a subsection is devoted to the introduction of Henry's constant (Section 5.3).

DOI: 10.1021/acsomega.9b02956
ACS Omega 2020, 5, 430−447

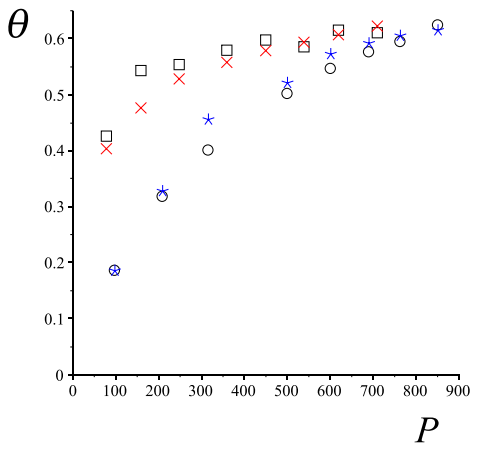

Figure 13. Circles and squares are the experimental data for adsorption (circles) and desorption (squares) of CH_4 by Wyoming coal at 295.15 K.[7] Blue asterisks (adsorption) and red crosses (desorption) result from model calculations. The horizontal axis gives pressure in PSI. The vertical axis gives dimensionless coverage.

A final section (Section 5.4) contains the derivation of the differential equation giving the rate of change of the coverage originating from eq 1.

5.1. Pressure and Spreading Pressure. As stated in the Introduction, it is assumed that the adsorbed fluid obeys a van der Waals equation of state. The two-dimensional van der Waals equation, used, for example, by Hoory and Prausnitz,[12] is used here

$$\Pi = \frac{N_\Sigma RT}{\Sigma - N_\Sigma \beta} - \frac{\alpha {N_\Sigma}^2}{\Sigma^2} \tag{25}$$

What follows is consistent when a monolayer is assumed. The maximum value of N_Σ is Σ/β so that the coverage is $N_\Sigma\beta/\Sigma$. The particle concentration and coverage are thus

$$c_\Sigma = N_\Sigma/\Sigma \tag{26}$$

$$\theta = \beta c_\Sigma \tag{27}$$

The critical values, identified by a subscript c, are expressed in terms of the constants α and β

$$\Pi_c = \frac{\alpha}{27\beta^2}, \qquad RT_{\Sigma c} = \frac{8\alpha}{27\beta} \tag{28}$$

Concerning the ambient fluid, three equations of state are considered: that of an ideal gas of type 0 (noninteracting zero-volume particles), that of an ideal gas of type 1 (noninteracting nonzero-volume particles), and a plain van der Waals equation

$$P^{\mathrm{id0}} = \frac{N_f RT}{V}, \qquad P^{\mathrm{id1}} = \frac{N_f RT}{V - N_f b},$$
$$P = \frac{N_f RT}{V - N_f b} - \frac{a {N_f}^2}{V^2} \tag{29}$$

Note that, in the type 0 and type 1 cases, one assumes that V is so large that $P^{\mathrm{id}\ 0}$ and $P^{\mathrm{id}\ 1}$ are valid approximations inside some pressure range, but that the van der Waals constants are different from zero, so that it makes sense to speak of critical pressure and temperature.

Ambient and adsorbed fluids are assumed to be at the same temperature T. Similar to the two-dimensional case above, one defines

$$c_f = N_f/V \tag{30}$$

$$r = bc_f \tag{31}$$

The critical values, identified by a subscript c, are expressed in terms of the constants a and b

$$P_c = \frac{a}{27b^2}, \qquad RT_{fc} = \frac{8a}{27b} \tag{32}$$

The critical temperatures of the ambient and adsorbed fluids have different notations because they are known to be different.

One now introduces a dimensionless temperature $\tilde{T}$, a dimensionless spreading pressure $\tilde{\Pi}$, and a dimensionless ambient pressure $\tilde{P}$, by

$$\tilde{T} = \frac{T}{T_{fc}}, \qquad \tilde{\Pi} = \frac{\beta\Pi}{RT_{fc}}, \qquad \tilde{P} = \frac{bP}{RT_{fc}} = \frac{P}{8P_c} \tag{33}$$

Consistently with the definition of $\tilde{T}$, one defines dimensionless critical temperatures for the ambient and adsorbed fluids

$$\tilde{T}_{fc} = 1, \qquad \tilde{T}_{\Sigma c} = \frac{T_{\Sigma c}}{T_{fc}} = \frac{\alpha}{a}\frac{b}{\beta} \tag{34}$$

It follows that

$$\tilde{\Pi}(\theta, \tilde{T}, \tilde{T}_{\Sigma c}) = \frac{\tilde{T}\theta}{1-\theta} - \frac{27}{8}\tilde{T}_{\Sigma c}\theta^2 \tag{35}$$

Similarly, the dimensionless versions of eq 29, are

$$\tilde{P}^{\mathrm{id0}}(r, \tilde{T}) = \tilde{T}r, \qquad \tilde{P}^{\mathrm{id1}}(r, \tilde{T}) = \frac{\tilde{T}r}{1-r},$$
$$\tilde{P}(r, \tilde{T}) = \frac{\tilde{T}r}{1-r} - \frac{27}{8}r^2 \tag{36}$$

The adsorbed and ambient molecules being chemically identical, α and β are related to a and b. If the gas molecules are spherical and isotropic before and after being adsorbed, then formulas giving α and β in terms of a and b exist[14] and result in $\tilde{T}_{\Sigma c} = 1/2$. Otherwise α and β, and thereby $\tilde{T}_{\Sigma c}$, are often determined by fitting theoretical results to experiments. Some examples of experimentally determined values for $\tilde{T}_{\Sigma c}$ are given in Table 1. It is assumed in the sequel that $\tilde{T}_{\Sigma c} < 1$.

Table 1. Values of $\tilde{T}_{\Sigma c}$ for the Indicated Adsorbates, on Graphite[a]

N_2	Ar	C_6H_6	$CHCl_3$	$CFCl_3$
0.36	0.46	0.14	0.39	0.43

[a]From Hoory and Prausnitz.[12]

Figure 14 defines the symbols used in this article concerning the ambient fluid (left) and the adsorbed fluid (right). In particular, θ_m and θ_M, which often occur, are easily obtainable as solutions of a cubic

$$\theta_{\frac{m}{M}} = \frac{2}{3}\left[1 - \cos\frac{\arccos(2\tau - 1) \pm \pi}{3}\right] \tag{37}$$

with

$$\tau = \frac{\tilde{T}}{\tilde{T}_{\Sigma c}}. \tag{38}$$

DOI: 10.1021/acsomega.9b02956
ACS Omega 2020, 5, 430−447

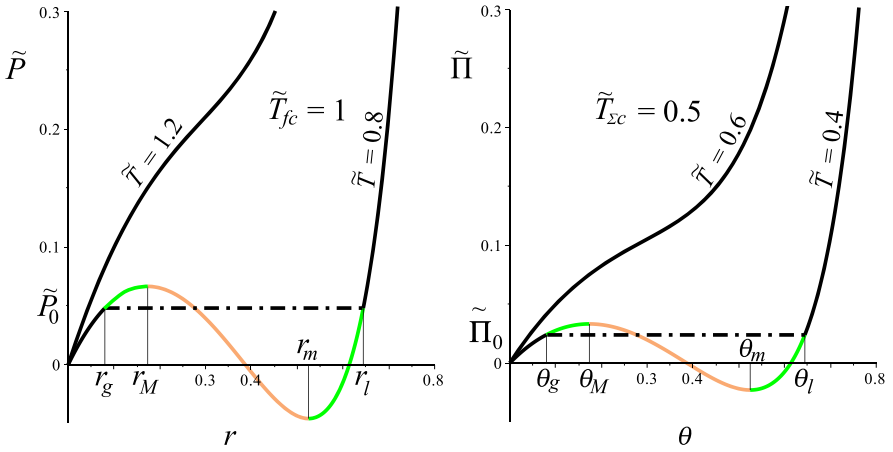

Figure 14. Left: Pressure $\tilde{P}(r,\tilde{T})$, eq 36 (right), for two values of $\tilde{T}$, one above and one below the critical value, $\tilde{T}_{fc} = 1$, vs r. Right: Spreading pressure $\tilde{\Pi}(\theta,\tilde{T},1/2)$, eq 35, for two values of $\tilde{T}$, one above and one below the critical value 1/2 vs θ. Concerning the similarity of the curves and also concerning the color and style of lines, see the text at the end of Section 5.1.

They are only defined when $\tau \leq 1$, that is, for a subcritical adsorbate. They satisfy $\theta_M \leq \theta_m$ (the equality occurring when $\tau = 1$) and are the abscissas of the intersections of the $\tilde{\Pi}(\theta,\tilde{T},\tilde{T}_{\Sigma c})$ versus θ curve with its spinodal curve: elsewhere in this article, θ_M and θ_m are referred to as the left and right spinodal coverages.

Figure 14 includes the known concepts of physical stability (black lines), physical metastability (green lines), and physical instability (orange lines). Equations of state represented by the black lines joined by the dash-dotted lines are called reconstructed.[17] A one-phase p-metastable state will eventually transit, at constant r (or constant θ for the adsorbate), to a two-phase p-stable state of lower energy on the reconstructed straight line.

The figure also illustrates the functional relationship implied by eq 35 and by the third of eq 36, namely: $\tilde{\Pi}(x,\tilde{T}_{\Sigma c}y,\tilde{T}_{\Sigma c}) = \tilde{T}_{\Sigma c}\tilde{P}(x,y)$.

5.2. Chemical Potentials and Fugacities. The chemical potentials can now be calculated, up to functions of temperature. The starting point is

$$\mathrm{d}F = -S\,\mathrm{d}T - P\,\mathrm{d}V + \mu_f\,\mathrm{d}N_f$$

One first obtains F by integrating at constant T and N_f; one then obtains μ_f by differentiating F with respect to N_f

$$\mu_f = \lim_{V^*\to\infty}\left(\left.\frac{\partial F}{\partial N_f}\right|_{T,V^*} + \int_V^{V^*}\left.\frac{\partial P}{\partial N_f}\right|_{T,V'}\mathrm{d}V'\right)$$

The limit when $V^* \to \infty$ of the first term inside the parenthesis on the right-hand side is the derivative with respect to N_f of the Helmholtz free energy of the ideal gas.[18] Using its expression, one gets

$$\mu_f = \lim_{V^*\to\infty}\left(RT\ln\frac{N_f\mathcal{V}(T)}{V^*} + \int_V^{V^*}\left.\frac{\partial P}{\partial N_f}\right|_{T,V'}\mathrm{d}V'\right) \quad (39)$$

where $\mathcal{V}$ has the dimension of molar volume. It can be obtained by the methods of statistical mechanics,[18] provided one has specific information about the properties of the molecules of the ambient fluid,[19] such as moments of inertia and vibrational frequencies. It is treated here as a function of T, referring to Section 5.3 for a further determination that involves Henry's adsorption constant. Performing the integration in eq 39, one finds that terms that diverge when $V^* \to \infty$ cancel, and one gets

$$\mu_f = RT\ln\frac{\mathcal{V}(T)}{b} + \mu_{f,red}(r,T) \quad (40)$$

The second term on the right-hand side, here named reduced chemical potential, has three alternative expressions, corresponding to the three alternative expressions for the pressure in eq 29

$$\mu_{f,red}^{id0}(r,T) = RT\ln r,$$

$$\mu_{f,red}^{id1}(r,T) = RT\ln\frac{r}{1-r} + RT\frac{r}{1-r},$$

$$\mu_{f,red}(r,T) = RT\ln\frac{r}{1-r} + RT\frac{r}{1-r} - \frac{27}{4}RT_{fc}r$$

The chemical potential of the adsorbed fluid is obtained by a similar method, μ_Σ being then given by a suitably modified right-hand side of eq 39: V, $\mathcal{V}$, P, and N_f being changed to A, $\mathcal{A}$, Π, and N_Σ. One gets

$$\mu_\Sigma = RT\ln\frac{\mathcal{A}(T)}{\beta} + \mu_{\Sigma,red}(\theta,T) \quad (41)$$

$$\mu_{\Sigma,red}(\theta,T) = RT\ln\frac{\theta}{1-\theta} + RT\frac{\theta}{1-\theta} - \frac{27}{4}RT_{\Sigma c}\theta \quad (42)$$

The fugacities f_f and f_Σ of the ambient and adsorbed fluids are now introduced, using the definition given by Hoory and Prausnitz,[12] written below in a form that is equivalent but slightly different from theirs

$$RT\ln f_f = \lim_{V^*\to\infty}\left(\int_V^{V^*}\left(\frac{\partial P}{\partial N_f}\right)_{T,V'}\mathrm{d}V' + RT\frac{N_f RT}{V^*}\right)$$

A similar formula applies for f_Σ where, in the right-hand side above, V, P, and N_f are changed to A, Π, and N_Σ. It is then easily shown that

DOI: 10.1021/acsomega.9b02956
ACS Omega 2020, 5, 430−447

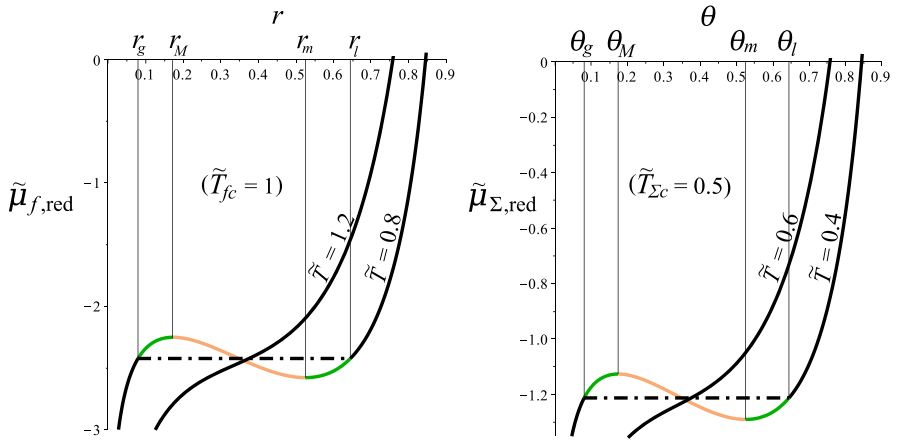

Figure 15. Left: Chemical potential $\tilde{\mu}_{\mathrm{f,red}}(r,\tilde{T})$, eq 49 (left), for two values of $\tilde{T}$, one above and one below the critical value, $\tilde{T}_{\mathrm{fc}} = 1$ vs r. Right: Chemical potential $\tilde{\mu}_{\Sigma,\mathrm{red}}(\theta,\tilde{T},1/2)$, eq 46 (left), for two values of $\tilde{T}$, one above and one below the critical value, $\tilde{T}_{\Sigma c} = 0.5$ vs θ. For both plots, the symbols on the axes and the colors of the lines are as defined in Figure 14. The dash-dotted lines are the reconstructed parts of the chemical potentials, see Figure 14.

$$\mu_{\mathrm{f}} = RT \ln \frac{\mathcal{V}(T)}{b} + RT \ln \frac{bf_{\mathrm{f}}}{RT},$$
$$\mu_{\Sigma} = RT \ln \frac{\mathcal{A}(T)}{\beta} + RT \ln \frac{\beta f_{\Sigma}}{RT}$$

Comparing these equations with 40 and 41, one obtains

$$\mu_{\mathrm{f,red}} = RT \ln \frac{bf_{\mathrm{f}}}{RT}, \qquad \mu_{\Sigma,\mathrm{red}} = RT \ln \frac{\beta f_{\Sigma}}{RT} \tag{43}$$

It is possible to show that one gets the expected result that Π and f_{Σ} become equal at the vanishing spreading pressure: according to eqs 26 and 27, $\Sigma = \beta N_{\Sigma}/\theta$ and letting $\Sigma \to \infty$ in eq 25, one gets $\Pi \approx RT\theta/\beta$. On the other hand, when $\theta \to 0$, then eq 42 shows that $\mu_{\Sigma,\mathrm{red}} \approx RT \ln \theta$ which, combined with eq 43, gives $f_{\Sigma} \approx RT\theta/\beta \approx \Pi$. It is similarly easy to show that $P \approx f_{\mathrm{f}}$ when $V \to \infty$.

It is convenient to introduce dimensionless chemical potentials and dimensionless fugacities to accompany the dimensionless pressures introduced in Section 5.1. The definitions are suggested by eqs 40−42 for the chemical potentials and by eq 43 for the fugacities

$$\tilde{\mu}_{\Sigma,\mathrm{red}} = \frac{\mu_{\Sigma,\mathrm{red}}}{RT_{\mathrm{fc}}}, \qquad \tilde{\mu}_{\mathrm{f,red}} = \frac{\mu_{\mathrm{f,red}}}{RT_{\mathrm{fc}}},$$
$$\tilde{f}_{\Sigma} = \frac{\beta f_{\Sigma}}{RT_{\mathrm{fc}}}, \qquad \tilde{f}_{\mathrm{f}} = \frac{bf_{\mathrm{f}}}{RT_{\mathrm{fc}}} \tag{44}$$

Equation 43 becomes

$$\frac{\tilde{f}_{\Sigma}}{\tilde{T}} = \exp \frac{\tilde{\mu}_{\Sigma,\mathrm{red}}}{\tilde{T}}, \qquad \frac{\tilde{f}_{\mathrm{f}}}{\tilde{T}} = \exp \frac{\tilde{\mu}_{\mathrm{f,red}}}{\tilde{T}} \tag{45}$$

One obtains, for the adsorbed fluid,

$$\tilde{\mu}_{\Sigma,\mathrm{red}}(\theta, \tilde{T}, \tilde{T}_{\Sigma c}) = \tilde{T} \ln \frac{\theta}{1-\theta} + \tilde{T}\frac{\theta}{1-\theta} - \frac{27}{4}\tilde{T}_{\Sigma c}\theta,$$
$$\tilde{f}_{\Sigma}(\theta, \tilde{T}, \tau) = \frac{\tilde{T}\theta}{1-\theta} \exp\left(\frac{\theta}{1-\theta} - \frac{27\theta}{4\tau}\right) \tag{46}$$

Similar expressions for the ambient fluid follow, where the particular cases of an ideal gas of type 0 or 1 are included:

$$\tilde{\mu}^{\mathrm{id0}}_{\mathrm{f,red}}(r, \tilde{T}) = \tilde{T} \ln r, \quad \tilde{f}^{\mathrm{id0}}_{\mathrm{f}}(r, \tilde{T}) = \tilde{T}r \tag{47}$$

$$\tilde{\mu}^{\mathrm{id1}}_{\mathrm{f,red}}(r, \tilde{T}) = \tilde{T} \ln \frac{r}{1-r} + \tilde{T}\frac{r}{1-r},$$
$$\tilde{f}^{\mathrm{id1}}_{\mathrm{f}}(r, \tilde{T}) = \frac{\tilde{T}r}{1-r} \exp \frac{r}{1-r} \tag{48}$$

$$\tilde{\mu}_{\mathrm{f,red}}(r, \tilde{T}) = \tilde{T} \ln \frac{r}{1-r} + \tilde{T}\frac{r}{1-r} - \frac{27}{4}r,$$
$$\tilde{f}_{\mathrm{f}}(r, \tilde{T}) = \frac{\tilde{T}r}{1-r} \exp\left(\frac{r}{1-r} - \frac{27r}{4\tilde{T}}\right) \tag{49}$$

Functions 46 and 49 are shown in Figure 15.

The following remarks refer to Figures 14 and 15.

1. Comparing eq 46 and the van der Waals version in eq 49, one sees that $\tilde{T}_{\Sigma c}\tilde{\mu}_{\mathrm{f,red}}(x,y) = \tilde{\mu}_{\Sigma,\mathrm{red}}(x,\tilde{T}_{\Sigma c}y,\tilde{T}_{\Sigma c})$ and Figure 15 illustrates this equality for $\tilde{T}_{\Sigma c} = 1/2$.
2. Figures 14 and 15 illustrate the following easily provable equalities:

$$\theta\frac{\partial}{\partial\theta}\tilde{\mu}_{\Sigma,\mathrm{red}} = \frac{\partial}{\partial\theta}\tilde{\Pi}, \qquad r\frac{\partial}{\partial r}\tilde{\mu}_{\mathrm{f,red}} = \frac{\partial}{\partial r}\tilde{P}$$

These show that the chemical potentials and the pressures, when plotted against their first argument, have local extrema at the same values of that argument. Also, the chemical potentials can be reconstructed by localizing the points with abscissas r_{g} and r_{l} (alternatively θ_{g} and θ_{l}), then replacing the loop between them by the horizontal straight line segment joining them. See Figure 15 where the lines have been drawn in the manner of Figure 14, with the same meanings.

It is assumed that the ambient fluid is constrained to always be in the same phase. There are no constraints on the adsorbed fluid, however, so that it can undergo a phase transition.

5.3. Henry's Adsorption Constant. Using eqs 40 and 41, an expression for the $\Delta\mu$ of eq 2 can now be written as

$$\Delta\mu/L = -RT \ln\left(\frac{\beta}{b}\frac{\mathcal{V}(T)}{\mathcal{A}(T)}\right) - \mu_{\mathrm{f,red}} + \mu_{\Sigma,\mathrm{red}} \tag{50}$$

The unknown function of T on the right-hand side is found by using the method used by Hoory and Prausnitz.[12] Using eq 43, eq 50 can be written as

DOI: 10.1021/acsomega.9b02956
ACS Omega 2020, 5, 430−447

$$\Delta\mu/L = -RT\ln\left(\frac{\beta}{b}\frac{\mathcal{V}(T)}{\mathcal{A}(T)}\right) - RT\ln\left(\frac{b}{\beta}\frac{f_f}{f_\Sigma}\right)$$

This formula remains valid when ambient gas and adsorbate are at equilibrium with each other at very low pressure: then, $\Delta\mu = 0$ and, according to the paragraph following eq 43, $f_\Sigma = \Pi = RTc_\Sigma$ and $f_f = P = RTc_f$. As the function of T does not depend on the physical situation, one obtains

$$RT\ln\left(\frac{\beta}{b}\frac{\mathcal{V}(T)}{\mathcal{A}(T)}\right) = -RT\ln\left(\frac{b}{\beta}\frac{c_f}{c_\Sigma}\right) \quad (51)$$

The pressure being low, the concentrations are small and c_Σ/c_f is Henry's adsorption constant, K_H. It is actually a function of temperature and of molecular properties, as defined in the literature that is used in this article.[20] It is convenient to introduce a dimensionless Henry constant, $\tilde{K}_H$, and the following expressions define the notation:

$$c_\Sigma = K_H c_f, \qquad \tilde{K}_H = \beta K_H/b \quad (52)$$

Then eq 51 gives

$$\frac{\beta}{b}\frac{\mathcal{V}(T)}{\mathcal{A}(T)} = \tilde{K}_H(\tilde{T}, \mathcal{D}) \quad (53)$$

where $\mathcal{D}$ is a set of constants that determine the interaction between adsorbent and adsorbate, and thereby the sorption properties.[20] Note that, with the notation introduced in eqs 31 and 27,

$$\theta = \tilde{K}_H r \quad (54)$$

when the pressure goes to zero.

Using eq 53 in eq 50 one obtains an expression for $\Delta\mu$ where the unknown function of temperature is replaced by Henry's "constant"

$$\Delta\mu/L = -RT\ln\tilde{K}_H(\tilde{T}, \mathcal{D}) - \mu_{f,red} + \mu_{\Sigma,red}$$

Introducing dimensionless chemical potentials by using the two first equations in the set 44, one obtains

$$\Delta\tilde{\mu} = \Delta\mu/(LRT_{fc}) \quad (55)$$

$$= \tilde{\mu}_{\Sigma,red}(\theta, \tilde{T}, \tilde{T}_{\Sigma c}) - \tilde{\mu}_{f,red}(r, \tilde{T}) - \psi(\tilde{T}, \mathcal{D}) \quad (56)$$

where

$$\psi = \tilde{T}\ln\tilde{K}_H(\tilde{T}, \mathcal{D}) \quad (57)$$

The dependence of ψ on a number of constants gathered in the set $\mathcal{D}$ implies that ψ can be seen as an experimental quantity that determines, at a given temperature, the adsorption properties of the combination of the fluid and adsorbing surface. See Section 4.

Experimental and theoretical results are cited below so as to establish an order of magnitude for the interval in which values of ψ are found.

K_H is usually written as $K_H = A_0\exp(T_0/T)$, where RT_0 is called the adsorption potential,[14] and A_0 is a function of T. An explicit expression for $A_0(T)$, in terms of a set of constants, is given in the framework of a model described by Dolgonosov.[20] The set $\mathcal{D}$ of constants is given by Dolgonosov[20] for 40 adsorbate molecules on a graphite adsorbent, and curves of K_H versus T are shown, together with experimental values, for selected temperature intervals. A selection of seven such curves is shown in Figure 16 (thin solid lines), covering a wide range of ψ-values. In addition, the five curves drawn with thick solid lines originate from data given in Ross and Olivier,[14] Finally, the broken line curve originates from data given by Saha et al.,[21] and the long thick solid line is the plot of Ψ_u defined by eq 8.

Figure 16 indicates that for temperatures and for adsorbate/adsorbent pairs that are industrially interesting, ψ is an approximately linear, slowly decreasing function of temperature, with numerical values roughly inside the interval 3 to 8. Values lower than 3 probably exist but characterize industrially uninteresting low adsorbers.

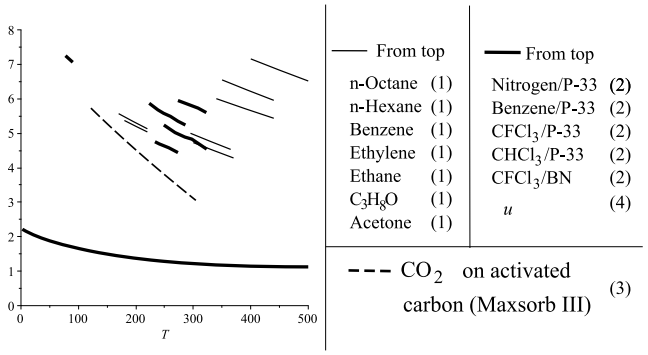

Figure 16. ψ vs T, from the sources indicated by the numbers in parentheses. (1) are from Dolgonosov;[20] (2) from Ross and Olivier,[14] where P-33 refers to graphitized carbon and BN to boron nitride; (3) from Saha et al.;[21] and (4) is eq 8.

5.4. Differential Equation for the Coverage. A differential equation for the coverage θ is here written by using eq 27 on the left-hand side of eq 1, eq 55 on its right-hand side, and then by introducing dimensionless time, $\tilde{t}$, by

$$\tilde{t} = \frac{t}{t_r}, \qquad \text{where } t_r = \frac{1}{L\beta RT_{fc}} \quad (58)$$

One obtains

$$\dot{\theta} = -\Delta\tilde{\mu}(\theta, r, \tilde{T}, \tilde{T}_{\Sigma c}, \psi) \quad (59)$$

where the dot on the left-hand side now denotes derivation with respect to $\tilde{t}$. In $\Delta\tilde{\mu}$ (see eq 56), $\tilde{\mu}_{f,red}$ is one of the three alternative equations given on the left-hand column of the set 47 to 49. The medium being homogeneous, and density being uniform, there is no space dependence, and eq 59 is to be solved in time, with an initial condition giving θ at time zero. The solution is sought for $\tilde{t} > 0$, and the coverage θ is in the interval (0, 1).

Most of this article is concerned with the equilibrium and the nonequilibrium solutions of eq 59, with the aim of determining their general characteristics. One is thus led to look at the solutions for different values of the parameters, so that it is important to know the intervals in which, in particular, t_r, $\tilde{T}_{\Sigma c}$, and ψ are likely to be in actual applications. Concerning $\tilde{T}_{\Sigma c}$ and ψ, see Sections 5.1 and 5.3, respectively.

Reference time t_r is unknown because of its dependence on L, a constant that, by definition, must be determined by dedicated experiments. As time-dependent results presented in this article are expressed in terms of dimensionless time, it is useful to have an order of magnitude for t_r. According to an article by Gleysteen and Deitz[22] published in 1945 on the sorption of nitrogen on carbon adsorbents, steady state is attained in about 20 min, meaning that sorption does not

DOI: 10.1021/acsomega.9b02956
ACS Omega 2020, 5, 430−447

measurably change for larger time values. More recently (1984), in Ruthven's book on adsorption,[23,24] sorption experiments of ethane on Linde 4A zeolite are cited, showing about the same time to steady state. Somewhat more extensive measurements were reported in 2010 by Battistutta et al.[8] on the sorption of methane, nitrogen, and carbon dioxide on dry coal. These showed that, to measure an equilibrium isotherm, the waiting time between pressure changes can vary between a day and 10 days, depending on the gas adsorbed and on temperature. It thus seems that values of t_r should be expected to be anything between a half hour and a week.

AUTHOR INFORMATION

Corresponding Author

*E-mail: paul.papatzacos@uis.no.

ORCID

Paul Papatzacos: 0000-0002-5193-4597

Notes

The author declares no competing financial interest.

ACKNOWLEDGMENTS

The author thanks Professor Aksel Hiorth for a number of clarifying discussions.

NOMENCLATURE

Latin Symbols

A, $A_{exp,i}$, coverage in SCF per ton, coverage of experimental point i on a graph in SCF per ton. See Section 4; $\mathcal{A}$, function of temperature and of molecular properties such as vibrational frequencies. It has the dimension of area per mole. See eq 41; a, b, van der Waals constants. See eq 29; c_Σ, c_f, number of adsorbed molecules per unit area (see eq 26), number of ambient molecules per unit volume (see eq 30); C, constant of dimension SCF per ton. See eq 21; C, in an adsorption experiment, estimated time used to compress the ambient gas from the lowest to the highest pressure, at a constant rate. See eq 22; $\mathcal{D}$, set of constants determining the interaction between adsorbate and adsorbent. See eq 53 and the statement following it; E_m, E_M, functions of τ introduced to define the vertical boundaries of the hysteresis loop. See eq 18; f_Σ, f_f, fugacities of the adsorbate and of ambient fluid. See Section 5.2; $\tilde{f}_\Sigma$, $\tilde{f}_f$, dimensionless fugacities of the adsorbate and ambient fluids. Defined in eq 44; $\tilde{f}_f^{id\ 0}$, $\tilde{f}_f^{id\ 1}$, dimensionless fugacities of the ideal ambient fluid with zero volume particles (superscript 0), or nonzero volume particles (superscript 1). See eq 47 (right) and 48 (right); F, Helmholtz free energy. See Section 5.2; K_H, $\tilde{K}_H$, dimensional and dimensionless Henry constant of adsorption. See eq 52; L, phenomenological constant. See eq 2; N_Σ, N_f, number of adsorbed moles on Σ (see eq 25), number of ambient moles in V (see eq 29); $P^{id\ 0}$, $P^{id\ 1}$, P, ambient fluid pressure for ideal fluid with zero volume molecules (superscript 0), with nonzero volume molecules (superscript 1), and for a van der Waals fluid. See eq 29; P_c, ambient fluid critical pressure. See eq 32 (left); $P_{exp,i}$, $\tilde{P}_{exp,i}$, pressure (PSI, dimensionless) of experimental point i. See Figure 10; $\tilde{P}^{id\ 0}$, $\tilde{P}^{id\ 1}$, $\tilde{P}$, dimensionless versions of $P^{id\ 0}$, $P^{id\ 1}$, P. See eq 33 (right); $\tilde{P}_0$, dimensionless saturation pressure. See Figure 14 (left); r, ratio of number of ambient molecules per unit volume to its maximum value. See eqs 30 and 31; r_e, equilibrium value of r, at a given ambient temperature and pressure; r_g, r_l, r-values for the saturated gas and saturated liquid, obtained through the Maxwell construction. See Figure 14; r_i, r_1, r_2, r-values locating the center of the hysteresis loop, its left- (subscript 1) and right-hand (subscript 2) vertical boundaries. See eqs 10 and 17; r_m, r_M, r-values of the local minimum or local maximum, of a van der Waals ambient fluid. See Figure 14 (left); r_c, r_f, parameters characterizing a compression-decompression cycle. See Figure 7; $r_{exp,i}$, r-value of experimental point number, i, such that $P(r_{exp,i}T_{exp}) = P_{exp,i}$. See Section 4 and Figure 10; $\overline{r}_k$, array of r-values. See Section 4, following eq 22; R, gas constant; S, entropy. See Section 5.2; t, $\tilde{t}$, t_r, time, dimensionless time, reference time. See eq 58; $\tilde{t}_d$, cycle duration, in a compression−decompression cycle. See Figure 7; $\overline{t}_k$, array of t-values. See Section 4, following eq 22; T, $\tilde{T}$, dimensional, dimensionless temperature. See eq 33; T_{exp}, $\tilde{T}_{exp}$, temperature at which a sorption measurement is carried out, its dimensionless counterpart; $T_{\Sigma c}$, T_{fc}, $\tilde{T}_{\Sigma c}$, $\tilde{T}_{fc}$, critical temperature of adsorbate fluid, of ambient fluid, and their dimensionless counterparts; v, rate of compression. See eq 22; V, volume variable in a three dimensional equation of state. See eq 29; $\mathcal{V}$, function of temperature and of molecular properties such as vibrational frequencies. It has the dimension of volume per mole. See eq 39

Greek Symbols

α, β, van der Waals constants. See eq 25; $\Delta\mu$, $\Delta\tilde{\mu}$, see eqs 1, 2, 59, and 56; θ, ratio of number of adsorbed molecules per unit area to its maximum value (coverage). See eq 27; θ_e, equilibrium value of θ, at a given ambient temperature and pressure; θ_m, θ_M, θ-values of the local minimum, or local maximum, of a van der Waals adsorbed fluid. See Figure 14 (right), and eq 37. θ_M and θ_m are also referred to as the left and right spinodal coverages; θ_{ea}, θ_{ed}, values of equilibrium coverage for a subcritical adsorbate. Subscript ea indicates the adsorption value, subscript ed indicates the desorption value. See eqs 11 and 12; μ_Σ, μ_f, chemical potential of the adsorbate and of ambient fluid. See Section 5.2; $\mu_{f,red}^{id\ 0}$, $\mu_{f,red}^{id\ 1}$, $\mu_{f,red}$, reduced chemical potential of the ideal ambient fluid with zero volume molecules (superscript 0), with nonzero volume molecules (superscript 1), and for a van der Waals fluid. See the three equations following eq 40; $\mu_{\Sigma,red}$, reduced chemical potential of the adsorbate. See eq 42; $\tilde{\mu}_{\Sigma,red}$, dimensionless reduced chemical potential of the adsorbate. See eq 46 (left); $\tilde{\mu}_{f,red}^{id\ 0}$, $\tilde{\mu}_{f,red}^{id\ 1}$, $\tilde{\mu}_{f,red}$, dimensionless reduced chemical potential of the ambient fluid for three cases: ideal fluid with zero volume molecules (superscript id 0), ideal fluid with nonzero volume molecules (superscript id 1), and van der Waals. See eqs 47−49 (left); Π, $\tilde{\Pi}$, spreading pressure of the adsorbate, dimensional (eq 25) and dimensionless (eq 35); $\tilde{\Pi}_0$, dimensionless saturation spreading pressure. See Figure 14 (right); Π_c, adsorbate critical pressure. See eq 28 (left); Σ, area variable in a two-dimensional equation of state. See eq 25; τ, see eq 38; ψ, function of temperature and of the set $\mathcal{D}$. Related to the Henry constant by eq 57; Ψ_w, Ψ_m, Ψ_M, functions of $\tilde{T}$ and $\tilde{T}_{\Sigma c}$, defined by eqs 8, 13, and 14. See also Figures 3 and 5

ADDITIONAL NOTES

[a]MAPLE's implicitplot has been used.

[b]Maple has been used, and the method of solution is rfk45, described as "Fehlberg fourth−fifth order Runge−Kutta".

REFERENCES

(1) Morishige, K.; Shikimi, M. Adsorption hysteresis and pore critical temperature in a single cylindrical pore. *J. Chem. Phys.* **1998**, *108*, 7821−7824.

DOI: 10.1021/acsomega.9b02956
ACS Omega 2020, 5, 430−447

(2) Hill, T. L. Statistical Mechanics of Multimolecular Adsorption. III. Introductory Treatment of Horizontal Interactions. Capillary Condensation and Hysteresis. *J. Chem. Phys.* **1947**, *15*, 767−777.
(3) Papatzacos, P.; Skjæveland, S. M. Relative Permeability From Thermodynamics. *SPE J.* **2004**, *9*, 47−56.
(4) Alfè, D.; Gillan, M. J. *Ab initio* statistical mechanics of surface adsorption and desorption. I. H_2O on MgO (001) at low covrrage. *J. Chem. Phys.* **2007**, *127*, 114709.
(5) Ball, P. C.; Evans, R. On the Mechanism for Hysteresis of Gas Adsorption on Mesoporous Substrates. *Europhys. Lett.* **1987**, *4*, 715−721.
(6) Zhao, H.; Lai, Z.; Firoozabadi, A. Sorption Hysteresis of Light Hydrocarbons and Carbon Dioxide in Shale and Kerogen. *Sci. Rep.* **2017**, *7*, 16209.
(7) Jessen, K.; Tang, G.-Q.; Kovscek, A. R. Laboratory and Simulation Investigation of Enhanced Coalbed Methane Recovery by Gas Injection. *Transp. Porous Media* **2008**, *73*, 141−159.
(8) Battistutta, E.; van Hemert, P.; Lutynski, M.; Bruining, H.; Wolf, K.-H. Swelling and sorption experiments on methane, nitrogen and carbone dioxide on dry Selar Cornish coal. *Int. J. Coal Geol.* **2010**, *84*, 39−48.
(9) Wang, K.; Wang, G.; Ren, T.; Cheng, Y. Methane and Carbon Dioxide sorption hysteresis on coal: A critical review. *Int. J. Coal Geol.* **2014**, *132*, 60−80.
(10) Papatzacos, P. Macroscopic Two-phase Flow in Porous Media Assuming the Diffuse-interface Model at Pore Level. *Transp. Porous Media* **2002**, *49*, 139−174.
(11) Myers, A. L.; Prausnitz, J. M. Thermodynamics of Mixed-Gas Adsorption. *AIChE J.* **1965**, *11*, 121−127.
(12) Hoory, S. E.; Prausnitz, J. M. Monolayer adsorption of gas mixtures on homogeneous and heterogeneous solids. *Chem. Eng. Sci.* **1967**, *22*, 1025−1033.
(13) Arrowsmith, D. K.; Pace, C. M. *Ordinary Differential Equations*; Chapman and Hall, 1982.
(14) Ross, J. P.; Olivier, S. *On Physical Adsorption*; Interscience Publishers, 1964.
(15) Olver, F. W. J.; Lozier, D. W.; Boisvert, R. F.; Clark, C. W. *NIST Handbook of Mathematical Functions*; National Institute of Standards and Technology and Cambridge University Press, 2010.
(16) Ang, W. T.; Garmón, F. A.; Khosla, P. K.; Riviere, C. N. Modeling Rate-Dependent Hysteresis in Piezo-Electric Actuators. *Proceedings of the 2003 IEEE/RSJ International Conference on Intelligent Robots and Systems*, 2003.
(17) Rowlinson, J. S.; Widom, B. *Molecular Theory of Capillarity*; Oxford University Press, 1982.
(18) Hill, T. L. *An Introduction to Statistical Thermodynamics*; Dover Publications, 1986.
(19) Papatzacos, P. The Helmholtz free energy of pure fluid substances and fluid mixtures. *Proceedings of the 8th International Conference on Heat Transfer, Fluid Mechanics and Thermodynamics*, 2011; pp 845−852.
(20) Dolgonosov, A. M. Calculation of Adsorption Energy and Henry Law Constant for Nonpolar Molecules on a Nonpolar Uniform Adsorbent. *J. Phys. Chem. B* **1998**, *102*, 4715−4730.
(21) Saha, B. B.; Jribi, S.; Koyama, S.; El-Sharkawy, I. I. Carbon Dioxide Adsorption Isotherms on Activated Carbons. *J. Chem. Eng. Data* **2011**, *56*, 1974−1981.
(22) Gleysteen, L. F.; Deitz, V. R. Hysteresis in the physical adsorption of nitrogen on bone char and other adsorbents. *J. Res. Natl. Bur. Stand.* **1945**, *35*, 285−307.
(23) Ruthven, D. M. *Principles of Adsorption and Adsorption Processes*; Wiley-Interscience Publications, 1984.
(24) Reference 23, Figure 6.5.

DOI: 10.1021/acsomega.9b02956
ACS Omega 2020, 5, 430−447